Journal of Proteomics 148 (2016) 213–227

Contents lists available at ScienceDirect

Journal of Proteomics

journal homepage: www.elsevier.com/locate/jprot

Ability of the marine bacterium *Pseudomonas fluorescens* BA3SM1 to counteract the toxicity of CdSe nanoparticles

Isabelle Poirier [a,*], Lauriane Kuhn [b], Arnaud Demortière [c,d,f], Boris Mirvaux [c,d], Philippe Hammann [b], Johana Chicher [b], Christelle Caplat [e], Marie Pallud [a], Martine Bertrand [a]

[a] Institut National des Sciences et Techniques de la Mer, Conservatoire National des Arts et Métiers, 50103 Cherbourg-Octeville Cedex, France
[b] Plateforme Protéomique Strasbourg Esplanade, CNRS FRC1589, Institut de Biologie Moléculaire et Cellulaire, 67084 Strasbourg Cedex, France
[c] Laboratoire de Réactivité et Chimie des Solides, CNRS UMR 7314, Université de Picardie Jules Verne, 80039 Amiens Cedex, France
[d] Réseau sur le Stockage Electrochimique de l'Energie (RS2E), CNRS FR 3459, 80039 Amiens Cedex, France
[e] UMR BOREA, UCBN, MNHN, UPMC, CNRS-7208, IRD-207, Institut de Biologie Fondamentale et Appliquée, Normandie Université, 14032 Caen Cedex 5, France
[f] Center for Nanoscale Materials, Argonne National Laboratory, 9700 South Cass Avenue, Argonne, IL 60439, United States

ARTICLE INFO

Article history:
Received 19 January 2016
Received in revised form 4 July 2016
Accepted 22 July 2016
Available online 11 August 2016

Keywords:
Marine bacteria
CdSe nanoparticles
Physiological responses
Proteomics
Oxidative stress

ABSTRACT

In the marine environment, bacteria from estuarine and coastal sediments are among the first targets of nanoparticle pollution; it is therefore relevant to improve the knowledge of interactions between bacteria and nanoparticles. In this work, the response of the marine bacterium *Pseudomonas fluorescens* BA3SM1 to CdSe nanocrystals (CdSe NPs) of 3 nm (NP3) and 8 nm (NP8) in diameter was evaluated through microscopic, physiological, biochemical and proteomic approaches. Transmission electron microscopy images showed that NP3 were able to penetrate the bacteria, while NP8 were highly concentrated around the cells, embedded in large exopolysaccharides. In our experimental conditions, both CdSe NP sizes induced a decrease in respiration during the stationary growth phase, while only NP8 caused growth retardation and a decrease in pyoverdine production. Proteomic analyses highlighted that the strain responded to CdSe NP toxicity by inducing various defence mechanisms such as cell aggregation, extracellular CdSe NP sequestration, effective protection against oxidative stress, modifications of envelope organization and properties, and cadmium export. In addition, BA3SM1 presented a biosorption capacity of 1.6×10^{16} NP3/g dry weight and 1.7×10^{15} NP8/g dry weight. This strain therefore appears as a promising agent for NP bioremediation processes. Proteomic data are available via ProteomeXchange with identifier PXD004012.

Biological significance: To the best of our knowledge, this is the first report focussing on the effects of CdSe colloidal nanocrystals (CdSe NPs) on a marine strain of *Pseudomonas fluorescens*. CdSe NPs are extensively used in the industry of renewable energies and it is regrettably expected that these pollutants will sometime soon appear in the marine environment through surface runoff, urban effluents and rivers. Bacteria living in estuarine and coastal sediments will be among the first targets of these new pollutants. The pseudomonads are frequently found in these ecosystems. They are involved in several biogeochemical cycles and are known for their high resistance to pollutants. Consequently, this study focussing on the effects of CdSe NPs on the marine strain *P. fluorescens* BA3SM1 is highly relevant for several reasons. First, it aims at improving knowledge about the interactions between bacteria and NPs. This is fundamental to effectively use NPs against pathogenic bacteria. Secondly, in spite of CdSe NP interactions with the bacterial cells, the strain BA3SM1 can develop various strategies to counteract CdSe NP toxicity and ensure its growth. It exhibits interesting properties to sequester CdSe NPs and it retains its ability to form biofilm. The strain therefore appears as a promising agent for NP bioremediation thanks to biofiltration processes. Finally, this study shows that CdSe NPs of 8 nm in diameter cause a decrease in the secretion of siderophore pyoverdine, a secondary metabolite playing a key role in microbial ecology since it drives bacterial survival and competitiveness in ecosystems. Bacteria producing effective siderophores survive better in a Fe-deficient environment where they antagonize the growth of other microbes thought iron deprivation. Furthermore, siderophores are also employed as virulence factors in human pathogenic strains such as *P. aeruginosa*. Consequently, this study highlights that NPs can impact the secondary metabolism of bacteria with environmental and medical implications.

Abbreviations: NPs, nanoparticles; CdSe NPs, cadmium-selenium colloidal nanocrystals; NP3, cadmium-selenium colloidal nanocrystals of 3 nm in diameter; NP8, cadmium-selenium colloidal nanocrystals of 8 nm in diameter; TOPO, trioctylphosphine oxide; ODPA, octadecylphosphonic acid; TOP, trioctylphosphine; AMM, acetate minimal medium; STEM, scanning transmission electron microscopy; HAADF, high angle annular dark field; ROS, reactive oxygen species; PBS, phosphate-buffered saline; DCFH-DA, dichlorofluorescein diacetate; RFU, relative fluorescens units; FDR, false-discovery rate; XIC, extracted ion chromatograms; PCA, principle component analysis; LPS, lipopolysaccharides.

* Corresponding author at: Institut National des Sciences et Techniques de la Mer, Conservatoire National des Arts et Métiers, France.
E-mail address: isabelle.poirier@cnam.fr (I. Poirier).

http://dx.doi.org/10.1016/j.jprot.2016.07.021
1874-3919/

In addition, in this work, Data-Dependant Acquisition (DDA) provided state of the art Mass Spectrometry data by Spectral Counting and MS1 Label-Free. The combination of these two well-known proteomic techniques including manual validations strengthened the identification and quantification of regulated proteins. Moreover, numerous correlations between proteomic analyses and other observations (physiological, biochemical, microscopic) consolidated our interpretations.

1. Introduction

In the past two decades, research efforts have resulted in the gradual introduction of nanoparticles (NPs) in numerous industrial fields, because of their unique optical, mechanical, electrical and magnetic properties (for a review, see [1]). Metallic NPs such as Quantum Dots (QDs) are fluorescent semiconductors composed of a metallic core and a surface layer of organic and/or inorganic molecules named shell. Among QDs, cadmium selenide (CdSe) QDs are the focus of numerous studies [2,3]. They have recently attracted attention as promising photovoltaic devices [4] and their use in solar panel design is expanding [5]. It is therefore regrettably expected that CdSe QDs will sometime soon appear in the marine environment through surface runoff, urban effluents and rivers, where their polluting power is unknown. To date, several studies regarding QD toxicity in different microorganisms have been published [6,7] but only a few of them have focussed on marine bacteria. QD toxicity depends on multiple factors derived from both inherent physicochemical properties and environmental conditions. QD size, charge, concentration, shell bioactivity, and oxidative, photolytic, and mechanical stability have each been implicated as determining factors in QD toxicity (for a review, see [8]). Several studies have also shown that the dissolution of the NP shell leads to a release of the metallic core and an increase in toxicity [9,10,11]. The toxicity of uncoated CdSe nanocrystals has been discussed in several reports and is associated, in part, with free cadmium released from the particle core [12,13]. For instance, Derfus et al. have demonstrated that the surface oxidation of CdSe nanocrystals, via air-induced and UV-catalyzed oxidation, results in the release of metal surface atoms and that the concentration of released cadmium directly correlates with cytotoxic effects [14]. In a recent study, the leaching behavior of CdSe particles was investigated [15]. They appeared to be stable in aqueous solutions but a marked enhancement in CdSe dissolution was confirmed at acidic and under aerobic conditions. Moreover, previous studies have shown that CdSe particles generate free radicals [16,17] and the free radical formation is considered as another primary mechanism for CdSe QD core toxicity (for a review, see [13]). Finally, CdSe nanocrystals can also cause membrane damage and penetrate into the cells where they induce intensive disturbances [18]; and their aggregation on the cell surface could impair cellular function [12].

In the marine environment, estuarine and coastal sediments are the main sink for various pollutants [19,20], therefore they will be particularly susceptible to NP pollution and bacteria which live in this specific environment will have to deal with these new pollutants. Among the bacteria surviving in polluted habitats, *Pseudomonas fluorescens* can follow major adaptation strategies [21,22]. In a previous study, the metal resistant bacterium *P. fluorescens* BA3SM1 was isolated from tidal flat sediments collected in a moderately metal-contaminated site to the west of Cherbourg seaport, France [23]. A proteomic analysis of the response of this marine strain to metallic ions showed that it acclimatizes by developing numerous defence mechanisms such as cell aggregation/biofilm formation, modification of envelope properties, decrease in metal uptake, metal export, protection against oxidative stress, metal sequestration and over-synthesis of proteins inhibited by metal [21]. In the literature, *P. fluorescens* was already used to produce NPs [24] but there is no study on the effect of uncoated CdSe nanocrystals on this species. Consequently, we chose to study the physiological and proteomic responses of *P. fluorescens* BA3SM1 to CdSe colloidal nanocrystals (CdSe NPs). This work, essential to understand the mechanisms developed by bacteria to counteract NP toxicity, will enable us to estimate the BA3SM1 strain's potential to immobilize these new pollutants, and therefore its potential to be used in NP bioremediation processes.

2. Materials and methods

2.1. Synthesis of CdSe colloidal nanocrystals

CdSe colloidal nanocrystals (CdSe NPs) of 3 nm and 8 nm in diameter (named, respectively, NP3 and NP8 in the manuscript) were used in this study. These two sizes were chosen because a previous study has demonstrated that the nanoparticles with a diameter in the range of 1–10 nm present a direct interaction with the bacteria [25]. In addition, they will display different degrees of toxicity based on their volume and metal content [25,26]. CdSe NPs were synthesized in a 50 mL three-neck flask using a Schlenk-line approach. TOPO (3.0 g, Sigma-Aldrich-99%), ODPA (0.308 g, PCI Synthesis-97%), and CdO (0.060 g, Sigma-Aldrich-99%) were mixed, heated up to 150 °C, and kept under vacuum for 2 h. The reaction solution was then heated up to 300 °C under nitrogen at approximately 7 °C/min. Next, 1.5 g of TOP was rapidly injected into the reaction flask. TOP-Se solution (0.058 g Se, Aldrich-98% + 0.360 g TOP, Sigma-Aldrich, 90%) was then also injected of 375 °C and 340 °C for the synthesis of NP3 and NP8, respectively. For NP3, the reaction was quenched 30 s after the TOP-Se injection by the injection of 5 mL of room-temperature toluene. For NP8, the reaction solution was kept at high temperature for 500 s. After the solution cooled down to room temperature, the CdSe NPs were precipitated by adding ethanol and centrifuging; this washing step was repeated twice. Finally, the CdSe NPs were re-dissolved in toluene and stored inside a glove box under nitrogen atmosphere. The size measurement of the newly synthesized pristine nanoparticles was based on a TEM image analysis using an automatic procedure (analyze particles) in the FIJI software. The study of their behavior in aqueous solution, by TEM image analysis, highlighted a satisfactory stability (good dispersion and no significant change in size). Scanning transmission electron microscopy (STEM) images of CdSe NPs are shown in Supplementary Fig. 1. The properties and characteristics of CdSe NPs are described in Supplementary Table 1.

2.2. Bacterial strain and growth conditions

P. fluorescens BA3SM1 was isolated and identified as described in a previous study [23]. It was deposited in the bacterial strain collection of the Institut Pasteur in France (CIP 110551). Long-term storage is carried out at −80 °C in 25% (v/v) glycerol. For all experiments, *P. fluorescens* BA3SM1 was cultivated at 20 °C with stirring (150 rpm) in acetate minimal medium (AMM) containing (g/L): NH_4Cl, 1.0; $MgSO_4 \cdot 7H_2O$, 0.2; $FeSO_4 \cdot 7H_2O$, 0.001; $CaCl_2 \cdot H_2O$, 0.001; sodium acetate, 5; yeast extract, 0.5; K_2HPO_4, 0.5 (pH 7). We had chosen to use a minimal culture medium to get closer to the nutritional conditions of the marine environment and because the pyoverdine production is higher under nutrient-poor conditions. Cultures (100 mL) were inoculated with bacterial suspensions from 24-h-old pre-cultures realized in nutrient broth at 20 °C, to obtain an initial cellular concentration of

about 10^5 cells/mL. The pre-culture allows reactivation of bacterial cells and the conduction of experiments with cells all in the same physiological and metabolic state.

To determine the effect of CdSe NPs on growth parameters, respiration, intracellular ROS level, pyoverdine secretion and proteome evolution of *P. fluorescens* BA3SM1, and to observe the interactions between CdSe NPs and bacteria, the AMM was supplemented with CdSe NPs of 3 nm in diameter (NP3) to obtain a concentration of 1.3×10^{16} NPs/L (1.1 mg/L; 23 nM), corresponding to an equivalent Cd concentration ([Cd]eq.) of 0.60 mg/L (5.3 μM) and an equivalent Se concentration ([Se]eq.) of 0.42 mg/L (5.3 μM) or with CdSe NPs of 8 nm in diameter (NP8) to obtain a concentration of 1.7×10^{15} NPs/L (2.7 mg/L; 3 nM), corresponding to a [Cd]eq. = 1.50 mg/L (13.5 μM) and a [Se]eq. = 1.10 mg/L (13.5 μM), immediately after the bacterial inoculation. These two concentrations provide similar exchange surface areas between NPs and bacterial cells ($3.5 \pm 0.2 \times 10^{17}$ nm^2/L) and therefore similar concentrations of surface metal atoms. Indeed, CdSe nanocrystal toxicity is mainly caused by the release of surface metal ions [14] and some authors claim that the main source of toxicity of these particles is not their metal content but rather the interaction of the particle surface with the cells [12]. Moreover, the study realized by Kirchner et al. demonstrated the relevance of using the surface atom concentration instead of the particle concentration [12]. Furthermore, these concentrations are high enough to induce metabolic changes in bacteria [26].

To study the effect of Cd^{2+} and Se^{2-} ions on the strain BA3SM1 (growth, intracellular ROS level and pyoverdine secretion) at concentrations corresponding to [Cd]eq. and [Se]eq. used during NP treatments, the AMM was supplemented with Cd or Se (atomic absorption spectrometry standard solutions, VWR International SAS, France) to obtain concentrations of 0.60 mg/L and 1.50 mg/L for Cd^{2+} and 0.42 mg/L and 1.10 mg/L for Se^{2-}.

2.3. Preparation of samples for STEM

Aliquots of 10 mL were removed from the NP-supplemented and control cultures at the beginning of the stationary growth phase (40-h-old cultures), freeze-dried and stored at −20 °C until STEM analysis. Ultrathin sections of samples embedded in epoxy resin were prepared as follows: in an Eppendorf tube, freeze-dried cells were re-hydrated and fixed for 1 h at 4 °C in water with 1% (v/v) glutaraldehyde, centrifuged (5500*g*, 10 min), rinsed three times in 10 mM HEPES (4-(2-HydroxyEthyl)-1-Piperazine Ethane Sulphonic acid) buffer (pH 7.5) and let in it for 3 h at 4 °C. They were then rinsed three times in distilled water, dehydrated in gradually increased ethanol/water relations until absolute ethanol and finally in acetone, with a centrifugation between each step. Still in the Eppendorf tube, dehydrated cells were progressively embedded in a mixture of acetone/epoxy resin (Epoxy, Fluka Chemica), centrifuged, then in full epoxy resin. To complete the polymerization, samples were then heated at 45 °C for 24 h, followed by 24 h at 60 °C. After a few days of air curing, resins were removed from the plastic tube and directly mounted on the sample holder of a RMC-PTXL ultramicrotome. Ultrathin sections (50–100 nm) were then cut with a RMC diamond knife (Inc. Angle 45°, setting 6°) equipped with a bath to receive the thin sections. Finally, they were recovered with a homemade perfect loop and dropped off on a STEM grid for observations. FEI Tecnai G2-F20 STEM was used to analyze ultrathin sections of samples.

2.4. Growth kinetics

NP-supplemented, metal ion-supplemented and control cultures were incubated at 20 °C with stirring (150 rpm). Growth was monitored by absorbance measurements at 600 nm (OD_{600}) using an APOLLO-1 microplate reader (Berthold Technologies), as described previously [21]. All experiments were performed in triplicate.

2.5. O_2 consumption measurement

O_2 consumption of the NP-supplemented and control cultures was measured with a Clark-type electrode as described in a previous study [27]. The measurements were performed at the beginning of the stationary growth phase (40-h-old cultures) with bacterial suspensions adjusted to the same concentration (6×10^8 cells/mL). All experiments were performed in triplicate.

2.6. Quantification of intracellular reactive oxygen species (ROS)

Intracellular ROS levels in cells from NP-supplemented, metal ion-supplemented and control cultures were measured using dichlorofluorescein diacetate (DCFH-DA) as described in a previous study [28], with minor modifications. Bacterial cells (1 mL) were pelleted by centrifugation for 10 min at 10,000*g* at 20 °C. The pellets were re-suspended with 1 mL phosphate-buffered saline (PBS) containing 30 μg/mL DCFH-DA dye, for 30 min at 20 °C in darkness with stirring (150 rpm). Then, the treated cells were re-pelleted (10 min at 10,000*g* at 20 °C) and re-suspended with 1 mL PBS. Intracellular ROS levels were quantified using an APOLLO-1 microplate reader (Berthold Technologies) by measuring fluorescence emission at 535 nm after excitation at 485 nm. The cell density of the corresponding cultures was determined by absorbance measurement at 600 nm and the results were expressed as relative fluorescence units (RFU)/cell. The measurements were performed from 14-h, 20-h, 40-h, 48-h and 62-h-old cultures for NP treatments and from 14-h, 20-h, 48-h and 62-h-old cultures for metal ion treatments. All experiments were performed in triplicate.

2.7. Pyoverdine quantification

Pyoverdine is a siderophore, a small organic molecule secreted by many microorganisms to chelate iron from the external environment in order to facilitate their growth and diverse metabolisms. Siderophores drive bacterial survival and competitiveness in the environment and they are significant factors for maintaining the habitats for most bacteria. Consequently, siderophores play a key role in microbial ecology and they are model metabolites to study the impact of NPs on bacteria (for a review, see [29]). Five milliliters of the NP-supplemented, metal ion-supplemented and control cultures were centrifuged for 10 min at 10,000*g* at 20 °C. The supernatants were filtered through 0.2 μm filters and pyoverdine was quantified using an APOLLO-1 microplate reader (Berthold Technologies) by measuring fluorescence emission at 460 nm after excitation at 405 nm. The cell density of the corresponding cultures was determined by absorbance measurement at 600 nm and the results were expressed as RFU/cell. The measurements were performed from 20-h, 32-h and 48-h-old cultures for NP treatments and for 20-h, 48-h and 62-h-old cultures for metal ion treatments. All experiments were performed in triplicate.

2.8. CdSe NP biosorption by P. fluorescens BA3SM1

The NP biosorption ability of *P. fluorescens* BA3SM1 was indirectly estimated by the measurement of the biosorbed Cd as described in a previous study [22]. Briefly, 12 mL aliquots were removed from the NP-supplemented and control cultures at the beginning of the stationary growth phase (40-h-old cultures) and centrifuged at 70,000*g* for 15 min at growth temperature with an OPTIMA L-100 XP ultracentrifuge (Beckman Coulter). The pellets were weighed, dried at 80 °C for 20 h, weighed again and digested with 5 mL 65% HNO_3 (Acros Organics). The digests were analyzed by atomic absorption spectrometry in flame mode with an AAS 240FS instrument (Varian). Controls without bacterial cells, treated in the same way, were done to quantify the amount of free CdSe NPs that sediment during the centrifugation step. These controls highlighted that, in the absence of bacterial cells, 15% of

NP3 and 57% of NP8 sediment during the centrifugation step. The measurements of biosorbed Cd were corrected accordingly. All the experiments were repeated in triplicate. Results were expressed as mg Cd biosorbed/g dry weight and as equivalent number of CdSe NPs biosorbed/g dry weight. Since the drying at 80 °C for 20 h removed only 93% of the water contained in the pellets (compared to drying at 103 °C for 24 h), the dry weights were corrected accordingly.

2.9. Proteomic analyses

2.9.1. Preparation of protein extracts

For protein extraction, NP-supplemented and control cultures were treated as described previously [27]. Protein extraction was performed from 40-h-old cultures. Briefly, after cell lysis with a French press (Thermo Scientific), the resulting homogenates were centrifuged for 1 h at 218,000*g* at 4 °C with an OPTIMA L-100 XP ultracentrifuge (Beckman Coulter) to pellet down cell debris. The supernatants, containing extracted proteins, were purified, concentrated, freeze-dried and stored at −20 °C until mass spectrometry analysis. For each culture condition (control, NP3 and NP8), protein extraction was performed in triplicate.

2.9.2. Mass spectrometry analysis

Protein extracts were quantified using a Bradford assay and prepared as described in a previous study [30]. Briefly, 5 μg of each sample were precipitated with 0.1 M ammonium acetate in 100% methanol, and proteins were re-suspended in 50 mM ammonium bicarbonate. After a reduction-alkylation step (dithiothreitol 5 mM - iodoacetamide 10 mM), proteins were digested overnight with sequencing-grade porcin trypsin (1:25, w/w). Half of the resulting vacuum-dried peptides were resuspended in 20 μL of water containing 0.1% (v/v) formic acid (solvent A). The peptide mixtures were analyzed using a NanoLC-2DPlus system (with nanoFlex ChiP module; Eksigent, ABSciex, Concord) coupled to a TripleTOF 5600 mass spectrometer (ABSciex) operating in positive mode. Five microliters of each sample (850 ng) were loaded on a ChIP C-18 precolumn (300 μm ID × 5 mm ChromXP; Eksigent) at 2 μL/min in solvent A. After 10 min of desalting and concentration, the pre-column was switched online with the analytical ChIP C-18 analytical column (75 μm ID × 15 cm ChromXP; Eksigent) equilibrated in solvent A:solvent B (95:5; v/v). Solvant B composition was formic acid:acetonitrile (0.1:100; v/v). Peptides were eluted by using a 5%–40% gradient of solvent B for 120 min at a flow rate of 300 nL/min. The TripleTOF 5600 was operated in data-dependant acquisition mode (DDA) with Analyst software (v1.6, ABSciex). Survey MS scans were acquired during 250 ms in the 350–1250 *m/z* range. Up to 20 of the most intense multiply charged ions (2+ to 5+) were selected for CID fragmentation, if they exceeded the 150 counts per second intensity threshold. Ions were fragmented using a rolling collision energy script within a 60 ms accumulation time and an exclusion time of 15 s. This so-called "Top20" method, with a constant cycle time of 1.5 s, was set in high-sensitivity mode.

2.9.3. Mass spectrometry-based quantification: spectral count approach

Data were searched against a *P. fluorescens* (strain Pf-5/ATCC BAA-477) database. The complete proteome set from the UniProt database (release from 2013-01-09, 12216 sequences) was added to human keratins and porcin trypsin sequences, and the final fasta file was created adding a decoy database (makeDecoyDB.pl, Bruker). The first algorithm used was Mascot (version 2.2, Matrix Science) through the ProteinScape 3.1 package (Bruker). Peptide modifications allowed during the search were: N-acetyl (protein), carbamidomethylation (C) and oxidation (M). Mass tolerances in MS and MS/MS were set to 20 ppm and 0.5 Da, respectively. Two trypsin missed cleavages sites were allowed. Peptide identifications obtained from Mascot were validated with *p*-value < 0.05 and proteins were validated respecting FDR < 1% (False-Discovery Rate). A Spectral Counting quantitative strategy was first carried on using the Mascot identification results and Proteinscape 3.1 package [31]: a spectral count value was first attributed to each protein and data were further normalized, by applying a correction factor to each condition according to the total spectra sum from each sample (the total spectra sum is ranging from 7370 spectra for control#3 to 9946 spectra for NP8#1). To list which proteins were regulated by the CdSe NP treatment (NP3 or NP8), we then averaged the number of spectra for each condition (control, NP3 and NP8) as they were analyzed as biological triplicates, and assigned a number of replicates per condition in which a given protein was identified and quantified. Finally, a ratio was calculated by dividing the average number of spectra obtained in the presence of CdSe NPs by the average number of spectra obtained in the control condition.

2.9.4. Mass spectrometry-based quantification: MS1 label-free approach

The Paragon algorithm (ProteinPilot package, AB Sciex) was then used to perform a second database search on the same nanoLC-MS/MS dataset and with the same decoy *P. fluorescens* database. Proteins validated by Paragon at FDR 1% were submitted to a MS1 label-free quantification. For that purpose, only non-modified and unshared peptides were considered, as well as the Paragon identification confidence threshold set at 99%. Precursor ions fulfilling these criteria were transferred into PeakView package (v 2.0 with Protein Quantitation plug-in, AB Sciex) and their corresponding eXtracted Ion Chromatograms (XIC) were automatically integrated, using the following parameters: RT window ±2 min, MS tolerance ±0.05 Da. To normalize and further process the MS1 label-free data, MarkerView software (v 1.2, ABSciex) was used: a correction factor was first applied to each condition according to the "Total Area Sum" function. The statistical module from MarkerView then allowed us to perform a Principle Component Analysis (PCA) and a Student *t*-test on the triplicate experiments from each of the 3 tested conditions (control, NP3 and NP8). Finally, two different tables were generated containing either the peptide areas or the protein areas: as for MS1 label-free quantification, we averaged the areas from triplicate injections and calculated the ratio by dividing the average area obtained in the presence of CdSe NPs by the average area obtained in the control condition.

A manual reconstruction of the peptides elution peaks was performed in a second instance, using the same software (PeakView, Sciex), to check whether the automatic integration process was being properly applied. A new ratio between NP supplemented and control conditions was calculated using average areas obtained by the manual reconstruction.

Only proteins presenting a sample/control ratio ≥ 1.5 or ≤0.67 for the three analysis (spectral count quantification, MS1-Label-Free quantification and manual reconstruction) were validated as regulated by CdSe NPs.

The mass spectrometric data were deposited to the ProteomeXchange Consortium via the PRIDE partner repository [32] with the dataset identifier PXD004012.

2.10. Statistical analysis

Results were expressed as means ± standard deviation of the triplicates. The Student *t*-test was used to know whether the mean values were significantly different between the different treatments at the $p \leq 0.05$ level. Statistical analysis was performed using R software version 3.2.0.

3. Results

3.1. STEM analyses of interactions between bacteria and CdSe NPs

The results of the STEM analyses are shown in Fig. 1. HAADF detector was used to acquire Z-contrast images so as to distinguish heavy elements (i.e. Cd and Se) (bright dots) and light elements of the bacteria. When *P. fluorescens* BA3SM1 was cultivated in NP3-supplemented

AMM, the CdSe NPs were clearly localized inside the cells, in the cell envelope, on the surface of the cell wall and also outside the cells embedded in extracellular organic compounds which were identified as exopolysaccharides (Fig. 1C and D). The NP3 were agglomerated to form big clusters (Fig. 1C and D, showed by blue arrows). When *P. fluorescens* BA3SM1 was cultivated in NP8-supplemented AMM, the CdSe NPs were mainly localized around the bacteria embedded in a large exopolysaccharide coat (Fig. 1E and F). Some NP8 were also localized in the cell envelope (Fig. 1E). Both CdSe NP sizes induced important envelope damage characterized by detachments of the plasma membrane from the cell wall (showed by red arrows). In the Fig. 1G–K, EDX analyses of NP8 immobilized by exopolysaccharides confirmed the presence of elements constituting NPs (Cd and Se) and polysaccharides (C). The detection of oxygen all over the EDX maps is explained by the presence of the resin used for preparing ultramicrotome TEM samples (Fig. 1G and J). P and Cl are two elements present in the AMM (Fig. 1K). Cu element is due to the TEM grid (Fig. 1K). Based on the electron diffraction pattern, NP8 are still crystalline with pristine structure (Wurtzite) even after interactions with bacterial cells (Fig. 1L). The Supplementary Fig. 2 shows numerous CdSe NPs immobilized by exopolysaccharides in 40-h-old bacterial cultures.

3.2. Effect of CdSe NPs on bacterial growth

The effect of CdSe NPs on the growth kinetics of *P. fluorescens* BA3SM1 cultivated in AMM at 20 °C is presented in Fig. 2. When *P.*

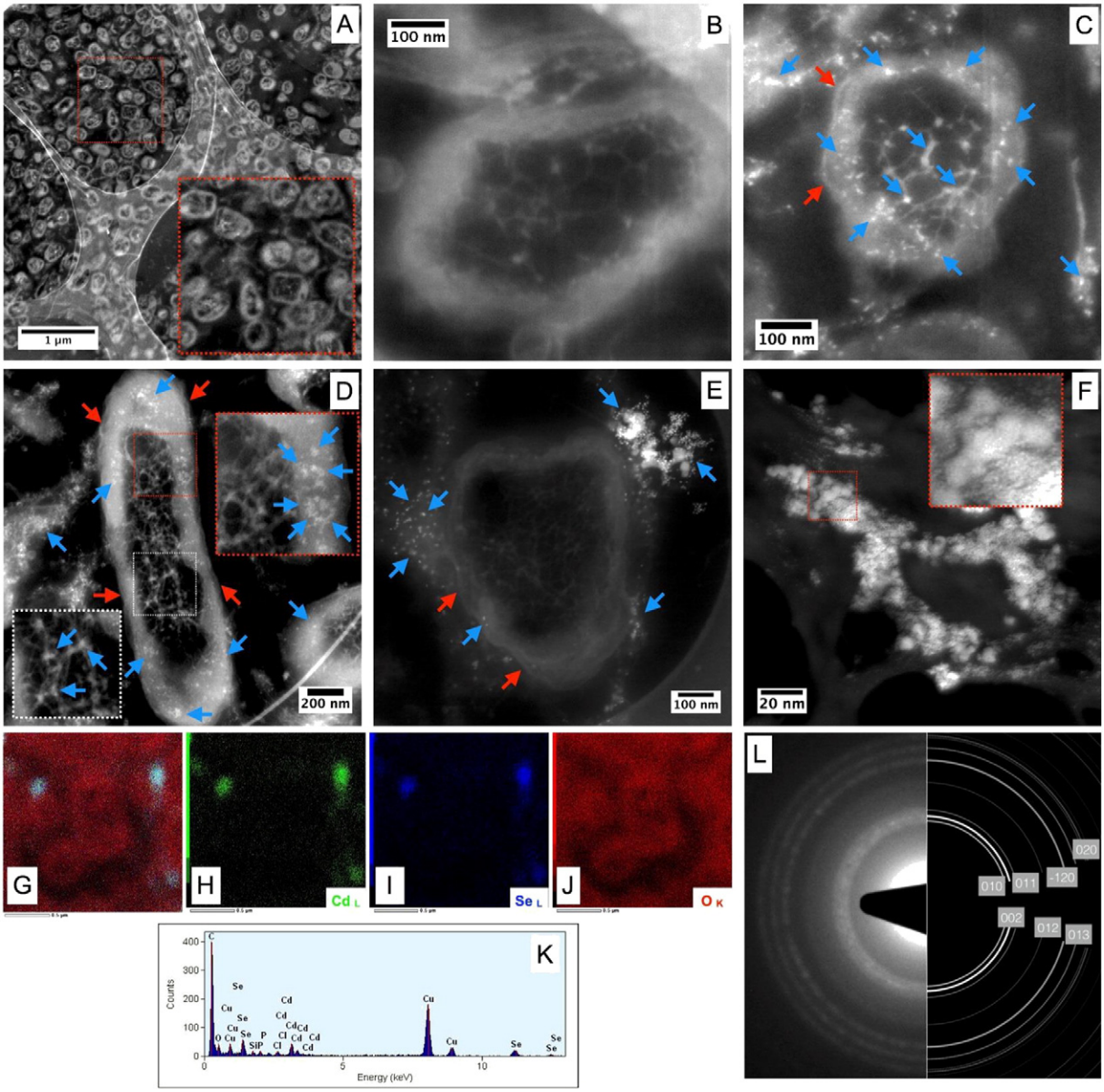

Fig. 1. STEM analysis. (A): HAADF-STEM image of an ultramicrotome-cut thin section of bacteria embedded in resin deposited on a carbon membrane. (B): HAADF-STEM image of individual bacterium cultivated in acetate minimal medium without CdSe colloidal nanocrystals (NPs). (C and D): HAADF-STEM image of individual bacterium cultivated in acetate minimal medium supplemented with NPs of 3 nm in diameter (NP3; 1.3×10^{16} NPs/L). Agglomerates of NP3 are localized inside the cell, in the cell envelope and outside the cell immobilized by exopolysaccharides (blue arrows). (E): HAADF-STEM image of individual bacterium cultivated in acetate minimal medium supplemented with NPs of 8 nm in diameter (NP8; 1.7×10^{15} NPs/L). NP8 are mainly localized around the bacteria embedded in exopolysaccharides (blue arrows). (F): HAADF-STEM image of NP8 (small white dots) embedded in a large exopolysaccharide coat. (G–J) EDX-STEM mapping of NP8 embedded in exopolysaccharides, respectively for the edges of Cd L, Se L and O K. (K) EDX-STEM spectrum associated with preview mapping. (L) Selected area electron diffraction pattern (Fig. 1F area) of NP8 (Wurtzite structure) after interaction with bacteria. Blue arrows point out NP3 and NP8. Red arrows point out envelope damage characterized by detachments of the plasma membrane from the cell wall.

fluorescens BA3SM1 was exposed to NP3 (1.3×10^{16} NP3/L, [Cd]eq. = 0.60 mg/L, [Se]eq. = 0.42 mg/L), a decrease in the lag phase was observed (about 4-fold), while the maximum growth rate (μ_{max}) and cell concentration were similar to the control ($\mu_{max} = 0.23 \pm 0.03$ h^{-1} and 0.21 ± 0.05 h^{-1} for control and NP3, respectively; cell concentration after 62 h of cultivation $= 3.1 \times 10^7$ cells/mL and 3.5×10^7 cells/mL for control and NP3, respectively). When *P. fluorescens* BA3SM1 was exposed to NP8 (1.7×10^{15} NP8/L, [Cd]eq. = 1.5 mg/L, [Se]eq. = 1.10 mg/L), a 1.5 fold increase was observed in the lag phase, as well as a slight decrease in the maximum cell concentration (2.6×10^7 cells/mL for NP8 instead of 3.1×10^7 cells/mL for the control). The μ_{max} was similar to that of the control.

During the growth, cell aggregations were observed with NPs, particularly with NP8 (Supplementary Fig. 3).

The impact of higher CdSe NP concentrations (2.6×10^{16} NPs/L, [Cd]eq. = 1.2 mg/L, [Se]eq. = 0.84 mg/L and 5.2×10^{16} NPs/L, [Cd]eq. = 2.4 mg/L, [Se]eq. = 1.68 mg/L for NP3; 3.4×10^{15} NPs/L, [Cd]eq. = 3 mg/L, [Se]eq. = 2.20 mg/L for NP8) on bacterial growth was also studied. All NP3 concentrations had the same positive impact on growth (a decrease in the lag phase), while 3.4×10^{15} NP8/L caused similar, but slightly more pronounced, negative impacts on growth (an increase in the lag phase and a slight decrease in the μ_{max}) than 1.7×10^{15} NP8/L. These results are shown in Supplementary Fig. 4. These additional results suggest that we must expose *P. fluorescens* BA3SM1 to very high CdSe NP concentrations (above 5.2×10^{16} NPs/L and 3.4×10^{15} NPs/L for NP3 and NP8, respectively) to strongly disturb its growth, in our experimental conditions.

3.3. Effect of CdSe NPs on bacterial respiration

The impact of CdSe NPs on the oxygen consumption of *P. fluorescens* BA3SM1 is presented in Fig. 3. When *P. fluorescens* was cultivated for 40 h with CdSe NPs, a decrease in oxygen consumption was observed. In our experimental conditions, the decrease in respiration was higher for NP8 (−51% compared to control, *t*-test: *p*-value = 0.01) than for NP3 (−43% compared to control, *t*-test: *p*-value = 0.04).

3.4. Effect of CdSe NPs on intracellular ROS levels

After 14 h of cultivation, high intracellular ROS levels were observed for the control and for NP8 ($>900 \times 10^{-5}$ RFU/cell), whereas this level was low for NP3 (29×10^{-5} RFU/cell) (Fig. 4A). After 20 h, the intracellular ROS level remained lower for NP3 than for the control and NP8, but values below 10×10^{-5} RFU/cell were observed for all culture conditions (Fig. 4B). After 40 h, 48 h and 62 h, the intracellular ROS levels remained below 10×10^{-5} RFU/cell with lower values for control (Fig. 4B). These results show a correlation between intracellular ROS level and growth. Indeed, the growth starts after a decrease in intracellular ROS level for all culture conditions.

3.5. Effect of CdSe NPs on pyoverdine secretion

When *P. fluorescens* BA3SM1 was cultivated in AMM without NPs, the pyoverdine secretion remained low after 20 h and 32 h of cultivation and increased remarkably (forty times) during the stationary phase (48-h-old culture) (Fig. 5). When *P. fluorescens* BA3SM1 was cultivated in AMM supplemented with NP3, no significant difference in pyoverdine secretion was observed (*t*-test: *p*-value > 0.05). However, in our experimental conditions, NP8 caused a high decrease in pyoverdine secretion (93%) during the stationary growth phase (48-h-old culture) (*t*-test: *p*-value ≤ 0.05) (Fig. 5).

3.6. Effect of Cd^{2+} and Se^{2-} ions on growth, intracellular ROS level and pyoverdine secretion

The impact of Cd^{2+} and Se^{2-} ions on the growth of *P. fluorescens* BA3SM1 is presented in Supplementary Fig. 5. Se^{2-} ions weakly impacted growth at 0.42 mg/L (a 1.2-fold increase in the lag phase and a 1.3-fold decrease in the μ_{max}), while they inhibited the cell growth at 1.1 mg/L (no growth occurred after 62 h of cultivation). Cd^{2+} ions induced cell growth disturbances such as an increase in the lag phase (approximately 2-fold and 3-fold at 0.60 mg/L and 1.5 mg/L, respectively) and a decrease in the maximal growth rate (0.24 h^{-1} for 0.60 mg/L and 0.18 h^{-1} for 1.5 mg/L instead of 0.43 h^{-1} for the control). The cell growth disturbances were stronger for 1.5 mg Cd/L than for 0.60 mg Cd/L.

The impact of Cd^{2+} and Se^{2-} ions on intracellular ROS levels is presented in Supplementary Fig. 6. After 14 h of cultivation, the

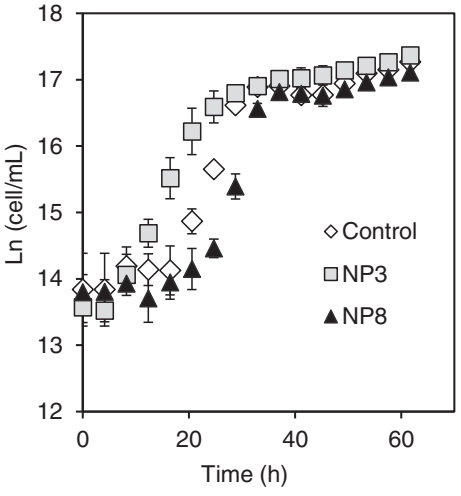

Fig. 2. Effect of CdSe colloidal nanocrystals on the growth of *P. fluorescens* BA3SM1. The strain was cultivated in acetate minimal medium without CdSe colloidal nanocrystals (control), with CdSe colloidal nanocrystals of 3 nm in diameter (NP3; 1.3×10^{16} NPs/L) or with CdSe colloidal nanocrystals of 8 nm in diameter (NP8; 1.7×10^{15} NPs/L). Data are means ± standard deviations (n = 3). Some standard deviations are not visible because they are shorter than the symbol size.

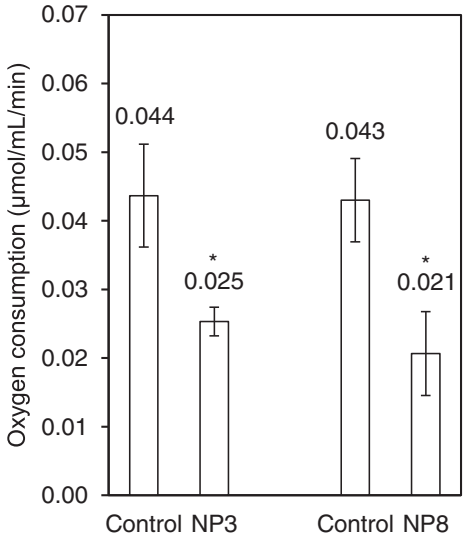

Fig. 3. Effect of CdSe colloidal nanocrystals on the respiration of *P. fluorescens* BA3SM1. The strain was cultivated in acetate minimal medium without CdSe colloidal nanocrystals (control), with CdSe colloidal nanocrystals of 3 nm in diameter (NP3; 1.3×10^{16} NPs/L) or with CdSe colloidal nanocrystals of 8 nm in diameter (NP8; 1.7×10^{15} NPs/L). The measurements were performed at the beginning of the stationary growth phase (40-h-old cultures) with bacterial suspensions adjusted to the same concentration (6×10^8 cells/mL). Data are means ± standard deviations (n = 3). The mean value of each bar with an asterisk (*) is significantly different from respective control according to Student *t*-test ($p \leq 0.05$).

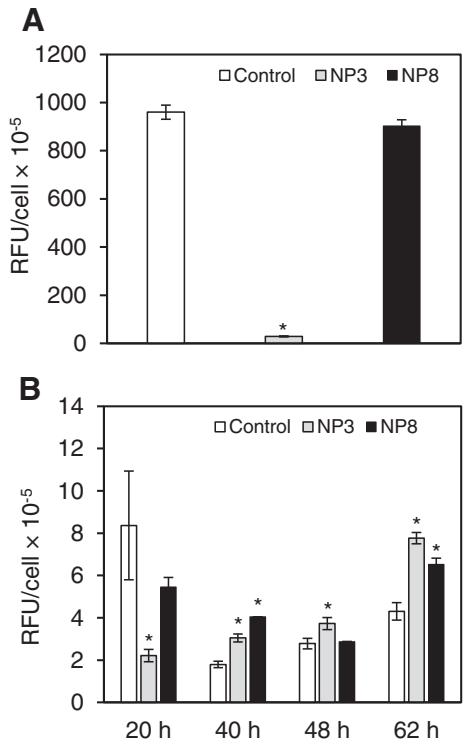

Fig. 4. Effect of CdSe colloidal nanocrystals on intracellular ROS level in *P. fluorescens* BA3SM1. The strain was cultivated in acetate minimal medium without CdSe colloidal nanocrystals (control), with CdSe colloidal nanocrystals of 3 nm in diameter (NP3; 1.3×10^{16} NPs/L) or with CdSe colloidal nanocrystals of 8 nm in diameter (NP8; 1.7×10^{15} NPs/L). (A): The measurements were performed from 14-h-old cultures. (B): The measurements were performed from 20 h, 40 h, 48 h and 62-h-old cultures. RFU = relative fluorescence units. Data are means ± standard deviations (n = 3). Some standard deviations are not visible because they are shorter than the symbol size. The mean value of each bar with an asterisk (*) is significantly different from respective control (control for the same time) according to Student *t*-test ($p \leq 0.05$).

intracellular ROS levels were higher for cells cultivated with 0.60 mg Cd/L, 1.5 mg Cd/L and 1.1 mg Se/L (>900×10^{-5} RFU/cell) than for control and cells cultivated with 0.42 mg Se/L (about 100×10^{-5} RFU/cell). Then, a decrease in intracellular ROS levels was observed over time to reach values of about 2×10^{-5} RFU/cell after 62 h for each treatment, except for 1.1 mg Se/L treatment where the intracellular ROS level remained high after 62 h (1000×10^{-5} RFU/cell). As for NP treatments, a decrease in intracellular ROS level seems necessary for the growth to begin.

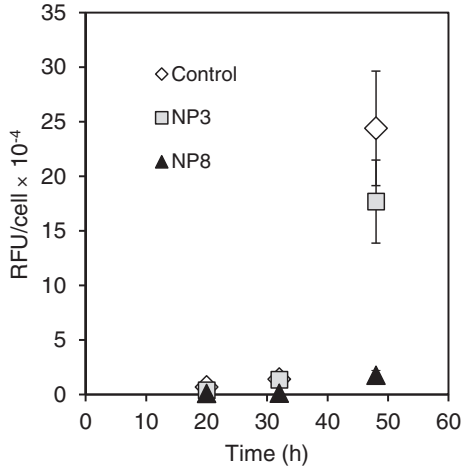

Fig. 5. Effect of CdSe colloidal nanocrystals on pyoverdine secretion by *P. fluorescens* BA3SM1. The strain was cultivated in acetate minimal medium without CdSe colloidal nanocrystals (control), with CdSe colloidal nanocrystals of 3 nm in diameter (NP3; 1.3×10^{16} NPs/L) or with CdSe colloidal nanocrystals of 8 nm in diameter (NP8; 1.7×10^{15} NPs/L). The measurements were performed from 20 h, 32 h and 48-h-old cultures. RFU = relative fluorescence units. Data are means ± standard deviations (n = 3). Some standard deviations are not visible because they are shorter than the symbol size.

The impact of Cd^{2+} and Se^{2-} ions on pyoverdine secretion is presented in Supplementary Fig. 7. When *P. fluorescens* BA3SM1 was cultivated in AMM supplemented with 0.42 mg Se/L, no significant difference in pyoverdine secretion was observed (*t*-test: *p*-value > 0.05) compared to the control. On the other hand, Cd^{2+} ions caused a strong decrease in pyoverdine secretion at the beginning of the stationary growth phase (54% with 0.60 mg Cd/L and 91% with 1.5 mg Cd/L) (*t*-test: *p*-value ≤ 0.05). When *P. fluorescens* BA3SM1 was cultivated in AMM supplemented with 1.1 mg Se/L, no pyoverdine secretion was observed during the experimentation.

3.7. Ability of P. fluorescens BA3SM1 to immobilize CdSe NPs from the medium

When *P. fluorescens* BA3SM1 was cultivated with NP3 for 40 h, the bacteria were able to immobilize 0.73 mg Cd/g dry weight, corresponding to an equivalent of 1.6×10^{16} NP3/g dry weight (Supplementary Fig. 8). When *P. fluorescens* BA3SM1 was cultivated with NP8 for 40 h, the bacteria were able to sequester 1.47 mg Cd/g dry weight, corresponding to an equivalent of 1.7×10^{15} NP8/g dry weight (Supplementary Fig. 8).

3.8. Differential protein expression

During the proteomic analyses, 1180 proteins were identified and among them 996 were quantified. Only proteins presenting a sample/control ratio ≥1.5 or ≤0.67 for both quantification strategies (spectral count and MS1-Label-Free quantification) and validated by manual reconstruction were considered as regulated by CdSe NPs. An illustration of the results obtained for both quantification strategies is shown in the Supplementary Fig. 9.

The proteomic analyses highlighted that NP3 induced the up-regulation of 13 proteins and the down-regulation of 18 proteins (Table 1), while NP8 induced the up-regulation of 22 proteins and the down-regulation of 44 proteins (Table 2). Proteins differentially expressed in the presence of CdSe NPs are involved in various biological processes such as metal resistance, transport and binding, genetic information processing, cell envelope biogenesis, TCA cycle, amino acid metabolism, fatty acid metabolism and other functions (protection against oxidative stress, oxidation-reduction processes, porphyrin synthesis, Fe—S cluster protein synthesis, protein maturation, polysaccharide and exopolysaccharide synthesis) (Fig. 6). NP3 mainly up-regulated proteins involved in oxidation-reduction processes (38%, all proteins classified in the "other functions" category) while NP8 mainly up-regulated proteins involved in amino acid metabolism (33%). Proteins down-regulated by NP3 are involved in four biological processes and mainly in genetic information processing (44%) while proteins down-regulated by NP8 are involved in eight biological processes and mainly in transport and binding (46%).

Two proteins were particularly over-synthesized with both sizes of CdSe NPs: the cadmium-exporting ATPase (average ratio >9 and 3 for NP3 and NP8, respectively) and the aminoethylphosphonate catabolism associated LysR family transcriptional regulator (average ratio >7 and 3 for NP3 and NP8, respectively) (Tables 1 and 2).

Characteristics of proteins regulated by CdSe NPs (MW, pI, Mascot score, sequence coverage, spectrum number, peptide area, *p*-value) are presented in Supplementary Tables 2 and 3.

4. Discussion

In this study, *P. fluorescens* BA3SM1 was exposed to NP3 and NP8 concentrations corresponding to a similar exchange surface area

Table 1
P. fluorescens BA3SM1 proteins differentially expressed from cells growing in the presence of CdSe colloidal nanocrystals (CdSe NPs) of 3 nm in diameter (1.3×10^{16} NPs/L).

Accession	Name	Ratio[a] (Spectral count quantification)	Ratio[a] (MS1-Label-Free quantification)	Ratio[a] (Manual reconstruction)	Function
		Up-regulated proteins (13)			
Metal resistance proteins					
Q4K483_PSEF5	Cadmium-exporting ATPase	9.79	10.33	15.13	Metal ion transmembrane transport
Transport/binding proteins					
Q4KBC9_PSEF5	Magnesium-importing ATPase	1.63	1.89	2.25	Magnesium ion transport; cation-transporting ATPase activity; metal ion binding
Q4K917_PSEF5	Cation ABC transporter, MZT family, ATP-binding protein	3.75	2.89	1.63	cation transport; ATPase activity
Genetic information processing					
Q4KIA2_PSEF5	Ribonuclease G	2.29	1.55	1.62	RNA processing; RNA binding
Q4K484_PSEF5	Aminoethylphosphonate catabolism associated LysR family transcriptional regulator	Absent in control	10.77	7.56	Regulation of transcription; sequence-specific DNA binding transcription factor activity
Cell envelope biogenesis					
Q4K603_PSEF5	Penicillin-binding protein 1B	Absent in control	2.81	1.92	Peptidoglycan biosynthesis; penicillin binding
Amino acid metabolism					
METE_PSEF5	5-methyltetrahydropteroyltriglutamate-homocysteine methyltransferase	Absent in control	1.49	2.56	Methionine biosynthesis
Fatty acid metabolism					
Q4K6D7_PSEF5	Putative medium-chain-fatty-acid: CoA ligase	2.16	1.92	2.11	Fatty acid metabolism; long-chain fatty acid-CoA ligase activity
Other proteins					
Q4KBL5_PSEF5	Dimethyl sulfone monooxygenase SfnG	1.66	1.77	1.71	Oxidation-reduction process
Q4KFP3_PSEF5	Electron transfer flavoprotein, alpha subunit	1.51	1.81	1.67	Oxidation-reduction process; electron carrier activity; flavin adenine dinucleotide binding
Q4KEZ1_PSEF5	FAD dependent oxidoreductase	1.79	1.57	1.54	Oxidoreductase activity
Q4KKN9_PSEF5	Luciferase family oxidoreductase, group 1	Absent in control	2.43	1.89	Oxidoreductase activity
Q4KHB1_PSEF5	Ferredoxin-NADP(+) reductase	1.61	1.55	2.02	Oxidation-reduction process; contribute to energy metabolism
		Down-regulated proteins (18)			
Transport/binding proteins					
Q4KHJ5_PSEF5	Efflux transporter, RND family, MFP subunit	0.24	0.59	0.22	Transmembrane transport
Q4KH22_PSEF5	Efflux transporter, membrane fusion protein subunit EmhA	0.67	0.54	0.31	Transmembrane transport
Q4KIZ3_PSEF5	TonB-dependent outermembrane copper receptor OprC	Present only in control	0.38	0.40	Copper, iron and heme transport
Q4KHV1_PSEF5	General L-amino acid ABC transporter, ATP-binding protein AapP	Present only in control	0.30	0.51	Amino acid transport; atpase activity
Genetic information processing					
RS21_PSEF5	30S ribosomal protein S21	0.55	0.30	0.12	Translation; structural constituent of ribosome
RS14_PSEF5	30S ribosomal protein S14	0.44	0.40	0.62	Translation; structural constituent of ribosome
RS19_PSEF5	30S ribosomal protein S19	0.45	0.04	0.17	Translation; structural constituent of ribosome
RS11_PSEF5	30S ribosomal protein S11	0.45	0.39	0.44	Translation; structural constituent of ribosome
RS12_PSEF5	30S ribosomal protein S12	0.59	0.36	0.32	Translation; structural constituent of ribosome
RS20_PSEF5	30S ribosomal protein S20	0.64	0.38	0.53	Translation; structural constituent of ribosome
RL11_PSEF5	50S ribosomal protein L11	0.65	0.25	0.66	Translation; structural constituent of ribosome
MUTS_PSEF5	DNA mismatch repair protein MutS	Present only in control	0.10	0.47	DNA repair; cellular response to DNA damage stimulus
Cell envelope biogenesis					
ARNC_PSEF5	Undecaprenyl-phosphate 4-deoxy-4-formamido-L-arabinose transferase	Present only in control	0.31	0.19	Lipid metabolic process; lipopolysaccharide biosynthesis; lipid A biosynthesis; response to antibiotic
Q4K609_PSEF5	CDP-diacylglycerol-serine O-phosphatidyltransferase	Present only in control	0.002	0.10	Phospholipid biosynthesis
Q4KDA2_PSEF5	Putative lipoprotein	Present only in control	0.06	0.27	
Others proteins					
Q4K4Q2_PSEF5	Formaldehyde dehydrogenase, glutathione-independent	0.52	0.53	0.49	Oxidoreductase activity; formaldehyde metabolism
Q4K6Z4_PSEF5	Siderophore-interacting protein family protein	0.51	0.61	0.29	Oxidoreductase activity
Q4KHQ0_PSEF5	Thiol:disulfide interchange protein DsbC	Present only in control	0.44	0.21	Protein folding; cell redox homeostasis

[a] Ratio between the NP supplemented and control conditions. Proteins on a grey background were differentially expressed with the two sizes of CdSe NPs.

Table 2
P. fluorescens BA3SM1 proteins differentially expressed from cells growing in the presence of CdSe colloidal nanocrystals (CdSe NPs) of 8 nm in diameter (1.7×10^{15} NPs/L).

Accession	Name	Ratio[a] (spectral count quantification)	Ratio[a] (MS1-Label-Free quantification)	Ratio[a] (manual reconstruction)	Function
		Up-regulated proteins (22)			
Metal resistance proteins					
Q4K483_PSEF5	Cadmium-exporting ATPase	9.59	2.99	12.10	Metal ion transmembrane transport
Transport/binding proteins					
HSLU_PSEF5	ATP-dependent protease ATPase subunit HslU	2.01	2.19	2.31	ATP binding; response to stress
Genetic information processing					
Q4KIB7_PSEF5	DNA-binding response regulator, Fis family	2.10	2.13	1.67	Phosphorelay response regulator activity; DNA binding
Q4K484_PSEF5	Aminoethylphosphonate catabolism associated LysR family transcriptional regulator	Absent in the control	5.13	3.75	Regulation of transcription; sequence-specific DNA binding transcription factor activity
Cell envelope biogenesis					
SURA_PSEF5	Chaperone SurA	1.50	2.28	1.64	Gram-negative-bacterium-type cell outer membrane assembly; protein folding; biofilm formation
Amino acid metabolism					
Q4K718_PSEF5	Aminotransferase, class III	1.94	4.24	5.61	Transaminase activity; pyridoxal phosphate binding
METE_PSEF5	5-methyltetrahydropteroyltriglutamate-homocysteine methyltransferase	Absent in the control	1.71	3.03	Methionine biosynthesis
Q4KEZ3_PSEF5	O-succinylhomoserine sulfhydrylase	2.28	2.62	2.78	Homocysteine biosynthesis
HISX_PSEF5	Histidinol dehydrogenase	1.85	2.61	2.20	Histidine biosynthesis
HIS81_PSEF5	Histidinol-phosphate aminotransferase 1	1.74	2.21	1.65	Histidine biosynthesis
GLYA1_PSEF5	Serine hydroxymethyltransferase	1.55	2.29	1.87	Glycine biosynthesis
Q4K5S2_PSEF5	Glutamate dehydrogenase	2.12	1.50	1.96	Cellular amino acid metabolic process; oxidation-reduction process
Other proteins					
Q4K5D7_PSEF5	Inorganic pyrophosphatase	1.56	2.00	2.50	Phosphate-containing compound metabolic process; magnesium ion binding
COAD_PSEF5	Phosphopantetheine adenylyltransferase	2.04	1.77	1.97	Coenzyme A biosynthetic process; nucleotidyltransferase activity
Q4KED6_PSEF5	Delta-aminolevulinic acid dehydratase	1.79	2.04	2.45	Porphyrin-containing compound biosynthetic process; tetrapyrrole biosynthetic process
DXR_PSEF5	1-deoxy-D-xylulose 5-phosphate reductoisomerase	Absent in the control	7.14	1.77	Terpenoid biosynthetic process; isoprenoid biosynthetic process; oxidation-reduction process
Q4K8B4_PSEF5	Cob(I)yrinic acid a,c-diamide adenosyltransferase	Absent in the control	2.16	2.06	Cobalamin biosynthesis
UBIB_PSEF5	Probable protein kinase UbiB	Absent in the control	4.44	1.77	Protein phosphorylation
HSCA_PSEF5	Chaperone protein HscA homolog	Absent in the control	3.00	1.78	Iron-sulfur cluster assembly; protein folding
Q4KC77_PSEF5	UDP-glucose 6-dehydrogenase	1.54	1.70	1.69	Polysaccharide biosynthetic process; oxidoreductase activity
Uncharacterized protein					
Q4KBM0_PSEF5	Uncharacterized protein	Absent in the control	2.34	6.78	
Q4K8L4_PSEF5	Uncharacterized protein	1.73	2.29	1.90	
		Down-regulated proteins (44)			
Transport/binding proteins					
Q4K4L3_PSEF5	Choline ABC transporter, periplasmic choline-binding protein	0.51	0.42	0.51	Choline binding and transport
Q4K3K6_PSEF5	Phosphate ABC transporter, periplasmic phosphate-binding protein	0.58	0.55	0.67	Transport
Q4KIZ3_PSEF5	TonB-dependent outermembrane copper receptor OprC	Present only in control	0.60	0.47	Copper, iron and heme transport
Q4KHV1_PSEF5	General L-amino acid ABC transporter, ATP-binding protein AapP	Present only in control	0.14	0.26	Amino acid transport; ATPase activity
Q4KAW5_PSEF5	Branched-chain amino acid ABC transporter, periplasmic branched-chain amino acid-binding protein	0.42	0.53	0.52	Amino acid transport
Q4KH87_PSEF5	Histidine ABC transporter, periplasmic histidine-binding protein HisJ	0.52	0.38	0.49	Histidine transport
Q4K798_PSEF5	Alpha-ketoglutarate MFS transporter KgtP	Present only in control	0.58	0.41	Transmembrane transport
Q4KFF8_PSEF5	Oxidoreductase, zinc-binding dehydrogenase family	0.47	0.19	0.55	Oxidoreductase activity; zinc ion binding
Q4KK62_PSEF5	TonB2 protein	Present only in control	0.32	0.63	Siderophore transmembrane transport
Q4K3H9_PSEF5	Putrescine-binding periplasmic protein	0.42	0.55	0.67	Polyamine binding and transport
Q4K435_PSEF5	Outer membrane porin OprE	0.50	0.41	0.51	Transmembrane transport
Q4K7C9_PSEF5	Outer membrane porin OprD	0.64	0.42	0.51	Transmembrane transport
Q4KK15_PSEF5	Taurine ABC transporter, periplasmic taurine-binding protein	0.55	0.35	0.66	Taurine transport
Q4KIU6_PSEF5	Type II/IV secretion system protein	Present only in control	0.23	0.33	Transport; ATP binding
Q4KJ43_PSEF5	Branched-chain amino acid ABC transporter, periplasmic branched-chain amino acid-binding protein LivJ	0.39	0.13	0.41	Amino acid transport
Q4K438_PSEF5	Aliphatic sulfonates ABC transporter, periplasmic sulfonate-binding protein	0.45	0.48	0.61	Sulfur compound transport and metabolism
Q4K8F4_PSEF5	Putative ABC transporter, periplasmic substrate-binding protein	0.36	0.35	0.46	
Q4KK45_PSEF5	D-methionine ABC transporter, periplasmic methionine-binding lipoprotein MetQ	0.50	0.32	0.46	Transport
Q4KG13_PSEF5	Periplasmic sulfate-binding protein	0.39	0.08	0.42	Sulfate transmembrane transport
Q4KK53_PSEF5	Putative amino acid ABC transporter, periplasmic amino acid-binding protein	0.44	0.07	0.51	Amino acid transport
Genetic information processing					
IHFA_PSEF5	Integration host factor subunit alpha	0.60	0.41	0.64	Regulation of transcription and translation
Q4KJK9_PSEF5	Poly(3-hydroxyalkanoate) granule-associated protein PhaF	0.21	0.06	0.23	Negative regulation of gene expression
Q4K3M3_PSEF5	DNA-binding protein HU, alpha subunit	0.14	0.10	0.58	Chromosome condensation
Cell envelope biogenesis					
Q4KHK8_PSEF5	OmpA family lipoprotein	0.30	0.31	0.23	Integral component of membrane

(continued on next page)

Table 2 (*continued*)

ARNC_PSEF5	Undecaprenyl-phosphate 4-deoxy-4-formamido-L-arabinose transferase	0.21	0.32	0.38	Lipid metabolic process; lipopolysaccharide biosynthetic process; Lipid A biosynthetic process; response to antibiotic
Q4K609_PSEF5	CDP-diacylglycerol-serine O-phosphatidyltransferase	Present only in control	0.00	0.60	Phospholipid biosynthetic process
Q4K5X5_PSEF5	Putative phospholipid-binding domain protein	0.39	0.19	0.24	
TCA cycle					
Q4K827_PSEF5	Acetyl-coenzyme A synthetase	0.37	0.29	0.33	Acetyl-CoA biosynthesis
Q4K3G8_PSEF5	Oxaloacetate decarboxylase alpha subunit	0.34	0.40	0.59	Oxaloacetate decarboxylase activity; lyase activity; sodium ion transport
Amino acid metabolism					
THIC_PSEF5	Phosphomethylpyrimidine synthase	0.08	0.27	0.06	Thiamine biosynthesis
Q4KDP4_PSEF5	2-oxoisovalerate dehydrogenase E2 component, dihydrolipoamide acyltransferase	0.18	0.62	0.60	Cellular amino acid catabolism
Fatty acid metabolism					
Q4KFU4_PSEF5	Acyl-coenzyme A dehydrogenase	0.14	0.56	0.45	Fatty acid beta-oxidation using acyl-CoA dehydrogenase; oxidation-reduction process
Others proteins					
Q4K4Q2_PSEF5	Formaldehyde dehydrogenase, glutathione-independent	0.05	0.19	0.24	Oxidoreductase activity; formaldehyde metabolism
Q4KKN8_PSEF5	Peroxiredoxin OsmC	0.61	0.05	0.37	Oxidation-reduction process; response to stress
Q4KK44_PSEF5	Monooxygenase, NtaA/SnaA/SoxA family	0.59	0.45	0.48	Oxidation-reduction process
Q4KIT6_PSEF5	Oxidoreductase, short chain dehydrogenase/reductase family protein	0.34	0.54	0.59	Oxidation-reduction process
Q4K439_PSEF5	Alkanesulfonate monooxygenase	0.30	0.39	0.54	Oxidation-reduction process
Q4K4X1_PSEF5	Protein kinase YeaG	0.44	0.25	0.39	protein phosphorylation
Q4KHQ0_PSEF5	Thiol:disulfide interchange protein DsbC	Present only in control	0.30	0.42	Protein folding; cell redox homeostasis
Q4KKK7_PSEF5	Catalase HPII	Present only in control	0.26	0.34	Response to oxidative stress; heme binding
Q4K436_PSEF5	Thiol-specific antioxidant protein LsfA	0.40	0.08	0.48	Oxidation-reduction process; antioxidant activity
Uncharacterized protein					
Q4K6D9_PSEF5	Uncharacterized protein	0.48	0.16	0.40	
Q4KI38_PSEF5	Uncharacterized protein	0.14	0.08	0.36	
Q4KKP2_PSEF5	Uncharacterized protein	0.07	0.24	0.31	

[a] Ratio between the NP supplemented and control conditions. Proteins on a grey background were differentially expressed with the two sizes of CdSe NPs.

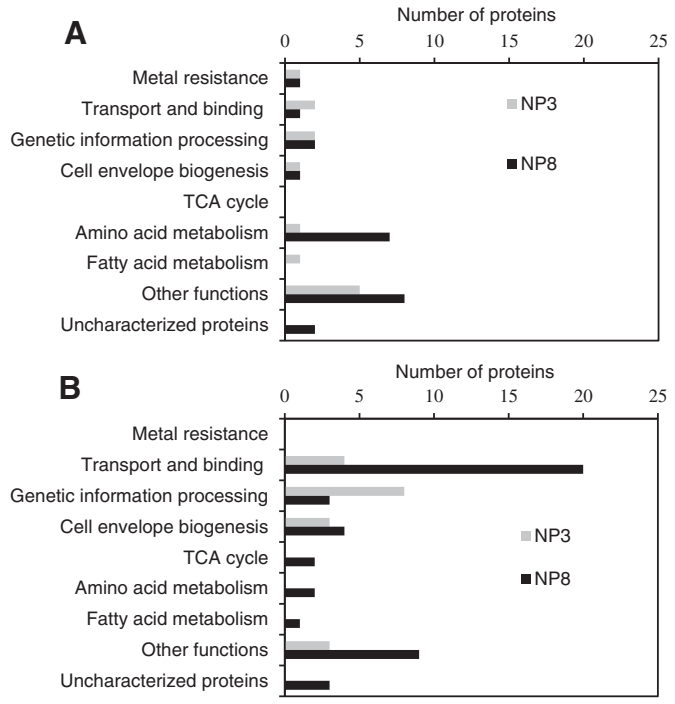

Fig. 6. Distribution of proteins regulated by CdSe colloidal nanocrystals based on the protein-associated biological processes. (A): Proteins up-regulated by CdSe colloidal nanocrystals of 3 nm in diameter (NP3; 1.3×10^{16} NPs/L) and 8 nm in diameter (NP8; 1.7×10^{15} NPs/L). (B): Proteins down-regulated by CdSe colloidal nanocrystals of 3 nm in diameter (NP3; 1.3×10^{16} NPs/L) and 8 nm in diameter (NP8; 1.7×10^{15} NPs/L). The x-axis represents the number of proteins for each biological process.

between NPs and bacterial cells for both treatments. Under these experimental conditions and after 40 h of cultivation, NP3 formed numerous agglomerates inside and outside the cells, while NP8 appeared still crystalline with pristine structure and very few agglomerated. A large amount of NP3 agglomerates and NP8 were embedded in exopolysaccharides. Moreover, the cell disorders induced by NPs were more numerous and more pronounced with NP8 than with NP3, e.g., a slight increase in the lag phase, a decrease in oxygen consumption, a high decrease in the pyoverdine secretion during the stationary phase and a differential expression of many proteins involved in transmembrane transport, cell envelope biogenesis and oxidation-reduction processes. Previous studies have shown that the Cd^{2+} release from the particle surface is one of the main mechanisms of CdSe NP toxicity [9,14,26,33,34], and that this process is enhanced by oxidation (air-induced and UV-catalyzed) [14] and acidic pH [9,15]. In our study, the Cd release from the NPs was confirmed by the high over-synthesis of the cadmium-exporting ATPase, and it was probably accompanied by a Se release. Unlike other studies on the impact of NPs on animal models in which metal ion release was quantified [35,36], our experimental conditions did not allow any such measurement. Indeed, in the presence of bacteria, the released metal ions may be immobilized by biosorption on bacterial wall and exopolysaccharides (Cd^{2+}) [37,38], by intracellular sequestration thanks to metalloproteins (Cd^{2+}) [39], or by incorporation in selenoproteins (Se^{2-}) [40], rendering difficult their recovery from the cultures. For example, in a previous study, we have shown that *P. fluorescens* BA3SM1 is able to biosorb up to 400 mg Cd^{2+}/g dry weight [22]. To our knowledge, the only study which presents results concerning the distribution of Cd^{2+} ions versus intact CdSe quantum dots (CdSe QDs) in bacterial cultures is that of Priester et al. [10]. These authors managed to quantify CdSe QD dissolution in bacterial cultures thanks to a complex methodology using several analysis techniques (inductively coupled plasma atomic emission spectroscopy (ICP-AES), X-ray absorption near edge spectra (XANES) and X-ray diffraction (XRD)). Interestingly, they have shown that CdSe QDs dissolved partially in growth media, but dissolution was lower in biotic cultures compared to sterile controls. In a more recent study, Monrás et al. also suggested that nanoparticle dismantling is impacted in the presence of bacterial cells [26]. Consequently, the interactions between *P. fluorescens* BA3SM1 and NPs, highlighted by STEM analyses, probably impacted NP dissolution, and it seems interesting, in further studies, to deepen our understanding of nanoparticle-bacteria interactions. To assess the amount of metal ions released from NPs, additional experiments were carried out to test the impact of Cd^{2+} and Se^{2-} ions on the strain BA3SM1 (growth, intracellular ROS and pyoverdine secretion) at concentrations corresponding to those imposed during NP treatments (0.60 mg/L and 1.5 mg/L for Cd, and 0.42 mg/L and 1.1 mg/L for Se). The impact of the different treatments applied (metal ion or CdSe NP enrichment) on bacterial cells (physiological and biochemical parameters) are synthesized in the Supplementary Table 4. These findings show that for similar metal concentrations, metal ions induced stronger growth disturbances and oxidative stress than CdSe particles. Therefore, we can assume that the amount of metal ions released from the NPs, in our experimental conditions, was low enough to allow bacteria to effectively counteract this pool of free ions. We can even hypothesize that the concentrations of free metal ions during NP treatments were below 0.42 mg/L and 0.60 mg/L for Se and Cd, respectively. The low NP dissolution is confirmed by STEM analyses which revealed the presence of numerous CdSe NPs in 40-h-old bacterial cultures. Interestingly, these results highlight that *P. fluorescens* BA3SM1 would probably be able to counteract the toxicity generated by a complete dissolution of the NP3, whereas a complete dissolution of the NP8 would have a lethal effect on this strain when it is cultivated in a minimal medium.

Cadmium (Cd^{2+}) represents an important source of toxicity. It can easily enter the bacterial cells and its toxicity might result mainly from the binding of Cd^{2+} to sulphide, thiol groups and sulphur-rich complex compounds [41]. Beside, several studies have shown correlations between the amount of Cd^{2+} released from CdSe NPs and their toxicity [9,12,36]. In our study, the high up-regulation of the cadmium-exporting ATPase gene expression highlights that *P. fluorescens* BA3SM1 counteracted CdSe NP toxicity by an active efflux of the released Cd^{2+}. Selenium (Se^{2-}) is an element that is essential in trace quantities but can also be toxic to bacteria [42]. At low concentrations, it can be readily oxidized into the nontoxic Se^0 and converted into seleno-amino acids (selenocysteine and selenomethionine) which are incorporated in the structure of several antioxidant defence proteins [40]. In our study, 0.42 mg Se/L had only a small effect on BA3SM1 (a slow decrease in growth), so the Se^{2-} released during NP treatments probably did not cause any harm to *P. fluorescens* BA3SM1. On the other hand, when this strain was submitted to 1.1 mg Se/L, strong negative effects were observed. These results suggest that the strain is unable to manage important Se pools in our experimental conditions (minimal culture medium and stirring), leading probably to a high accumulation of toxic selenium oxyanions in the culture medium. Similar observations were mentioned by Bebien et al. [43]. In previous studies on CdSe NP toxicity, the involvement of the released Se was rarely studied. However, our results show that this element can be more toxic than Cd for bacteria.

Several previous studies have also demonstrated CdSe NP toxicity independently of the metal being released. For instance, Kirchner et al. suggested that the aggregation of CdSe NPs on the cell surface could impair cellular function [12]. Other authors mentioned that NPs with a diameter of 1–10 nm are able to attach to the surface of the cell envelope and penetrate the bacteria [25], leading to drastic disturbances such as the loss of membrane integrity [10,26]. In our study, the location of NP8 into the cell envelope and extensively around the cells probably affects essential cellular functions, such as transmembrane transport. NP3 were localized inside and outside the cell, and STEM analysis highlighted their agglomeration. This agglomeration may decrease the release of

metal ions by creating larger particles with fairly low surface to volume, as it was demonstrated in a previous study [9]. NP3 agglomeration could be caused by culture medium properties, as observed in other studies [28,34], or/and by NP-bacteria and NP-exopolysaccharides interactions. Hence, further study should be conducted to deepen our understanding of nanoparticle-bacteria interactions and to elucidate mechanisms by which these interactions can cause NP agglomerations.

In the following paragraphs, we will discuss the main cell disturbances induced by CdSe NPs and the strategies developed by *P. fluorescens* BA3SM1 to fight their toxicity.

4.1. Growth – intracellular ROS level and oxidative stress

Our results have shown that the bacterial cells have to decrease their intracellular ROS level to start growing. At the beginning of the cultures, the intracellular ROS accumulation and oxidative stress can be generated by two phenomena: the modifications of the culture conditions between pre-cultures and cultures (pre-cultures were realized in a rich broth without stirring whereas cultures were realized in a minimal medium with stirring) and the presence of CdSe NPs. The modification of growth conditions is perceived as a stress by bacteria which induces oxidative-stress regulons [44], and CdSe NP toxicity is frequently associated with ROS accumulation and oxidative stress, generated mainly by the metal ion release [28,33] and the free radical generation [16,17]. In our study, metal ion release from CdSe NPs being confirmed by the up-regulation of the cadmium-exporting ATPase gene expression, NP treatments certainly generated an additional oxidative stress for bacteria. Nevertheless, after 14 h of cultivation, metabolic changes induced by NP3 helped the bacteria to decrease the intracellular ROS level more effectively than the control and therefore to grow faster, while metabolic changes induced by NP8 prevented an increase in intracellular ROS level. In the presence of NP3, the decrease in the intracellular ROS level was probably facilitated by the up-regulation of several proteins involved in the protection against oxidative stress (e.g., FAD dependent oxidoreductase; luciferase family oxidoreductase; ferredoxin-NADP(+) reductase; dimethyl sulphone monooxygenase SfnG; electron transfer flavoprotein) could explain the low intracellular ROS level observed for 14-h-old cultures. The ferredoxin-NADP(+) reductase is a committed member of the *sox*RS regulatory system involved in superoxide resistance in *Escherichia coli* [45] and protection against metal stresses [46]. The bacterial luciferase is known to play a fundamental role in the protection against oxidative stress [47]. In the presence of NP8, the fight against the oxidative stress and therefore the growth were probably slowed down by the down-regulation of numerous proteins involved in the transmembrane transport of nutrients and protection against oxidative stress (Table 2). To compensate for this disadvantage, *P. fluorescens* BA3SM1 has to adapt its metabolism during the prolonged lag phase which represents the rejuvenation of bacterial life that accompanies the development of the intracellular macromolecular stores needed for optimal growth [48]. However, after 20 h of cultivation, the strain managed to effectively combat oxidative stress generated by NP8, probably thanks to the up-regulation of several proteins involved in the synthesis of amino acids constituting metallothioneins and glutathione (histidine, glycine, glutamate and cysteine). Metallothioneins act as chelating agents for the excess of metals and hence help prevent oxidative stress in cells [49]. Glutathione is considered a major ROS scavenger with a key role in antioxidant defence [50]. Thus, *P. fluorescens* BA3SM1 managed to preserve a key tool against oxidative stress, while NP exposure caused glutathione depletion in other bacteria as *Pseudomonas putida* [7] and *E. coli* [28]. Moreover, under NP8 stress, oxidative stress was probably reduced by the up-regulation of proteins implicated in the porphyrin synthesis (delta-aminolevulinic acid dehydratase) or iron-sulphur cluster assembly and protein folding (chaperone protein HscA homolog) (Table 2). Indeed, an over-synthesis of porphyrin probably allowed the bacterial cells to produce high level of catalase HPI, which is especially effective at higher doses of H_2O_2 [51]. And the over-synthesis of proteins involved in iron-sulphur cluster assembly and protein folding suggests an over-synthesis of the [2Fe—2S] cluster containing SoxR protein. SoxR senses oxidative stress using the redox states of the [2Fe—2S] cluster and activates the transcription of the *soxS* gene, a transcription factor that promotes the production of various antioxidant proteins, including superoxide dismutase and the outer-membrane drug efflux TolC (for a review, see [52]).

In our study, the protection against oxidative stress induced by CdSe NPs was also provided by the high up-regulation of the cadmium-exporting ATPase and aminoethylphosphonate catabolism associated LysR family transcriptional regulator. The cadmium-exporting ATPase allows an active efflux of released Cd^{2+}, thereby decreasing oxidative stress generated by these free ions. This result is in accordance with a previous study showing an over-synthesis of a metal efflux pump in *E. coli* submitted to CdTe-GHS QDs [26]. LysR-type transcriptional regulators activate the transcription of genes coding for essential proteins implicated against oxidative stress such as the electron shuttle flavodoxins (Flds) [53]. In addition, the two sizes of NPs induced an up-regulation of proteins involved in homocysteine and methionine biosynthesis, (e.g., o-succinylhomoserine sulphhydrylase; 5-methyltetrahydropteroyltriglutamate-homocysteine methyltransferase; cob(I)yrinic acid a,c-diamide adenosyltransferase). This result seems to suggest that *P. fluorescens* BA3SM1 was able to use released selenium to synthesize selenoproteins which are involved in the oxidative stress response such as glutathione peroxidase [54].

As a consequence, resistance mechanisms developed by *P. fluorescens* BA3SM1 to combat oxidative stress generated by NPs ensure a lasting protection to cells, even during the stationary phase which is known to induce numerous stresses and cellular changes [55]. However, an increase in ROS production under NP stress is not systematic. Indeed, several studies have shown the efficiency of surface coatings such as polyethylene oxide [36] or polyethylene glycol [9] to avoid metal ion release from NPs and thus oxidative stress. For example, CdTe-Glutathione Quantum Dots of 3 nm did not allow an increase in ROS production in *E. coli* [26].

Unlike CdSe NPs which did not cause an increase in intracellular ROS level after 14 h of cultivation compared to the control, significantly enhanced intracellular ROS levels above that of the control were observed with Cd^{2+} (0.60 mg/L and 1.5 mg/L) and Se^{2-} (1.1 mg/L) causing lag phase prolongation for Cd and complete loss of culturability for Se. These results show that metal ions in nanoparticulate form generate lower oxidative stress than free metal ions, at equivalent mass concentrations. Similar results were also reported in previous studies [36,56].

4.2. Cell aggregation - extracellular NP sequestration

In our study, the up-regulation of some proteins such as the chaperone SurA (with NP8), penicillin-binding protein 1B (with NP3) and UDP-glucose-6-dehydrogenase (with NP8) suggests that *P. fluorescens* BA3SM1 was able to counteract NP toxicity by forming cell aggregates and sequestering NPs on polysaccharides. Indeed, the chaperone SurA and the penicillin-binding protein 1B are involved in biofilm formation [57,58] while the UDP-glucose-6-dehydrogenase generates UDP-glucuronic acid, a substrate in the production of many bacterial surface glycostructures [59]. The cell aggregation observed in the presence of NPs (Supplementary Fig. 3) and the extracellular NP sequestration revealed by STEM images (Fig. 1) support this hypothesis. These results are in accordance with previous studies showing that the cell aggregation and extracellular sequestration are strategies frequently developed by bacteria to resist metallic pollutants [10,21,60]. However, NPs were also responsible for biofilm inhibition in several studies [6,61]. Consequently, *P. fluorescens* BA3SM1 exhibits interesting properties to immobilize NPs, as it is now recognized that environmental biofilms are efficient binding matrices for NPs (for a review, see [62]).

In our study, *P. fluorescens* BA3SM1 was able to immobilize 0.73 mg Cd/g dry weight in the presence of NP3 and 1.47 mg Cd/g dry weight in

the presence of NP8. If the biosorbed Cd is totally in nanoparticulate form, these results suggest that the strain was able to sequester 1.6×10^{16} NP3/g dry weight and 1.7×10^{15} NP8/g dry weight, corresponding to 39% and 29% of the NP3 and NP8 added in the culture medium, respectively. In the literature, only a few studies focus on the use of microorganisms to remove NPs from environment, and fungi are described as being more efficient than bacteria. For instance, the bacterium *Aeromonas punctate* immobilized only 15% of the Ag NPs added in the culture medium [63], while *Pleurotus eryngii* and *Trametes versicolor* mycelia were able to sequester 86% and 61% of the Al_2O_3 NPs present in their environment, respectively [64]. *P. fluorescens* BA3SM1 is then the first promising bacterial candidate for removing NPs from contaminated waters using biofiltration prototypes proposed in recent studies [65,66].

4.3. Respiration - pyoverdine secretion - organization and properties of cell envelope

After 40 h of cultivation (beginning of the stationary growth phase), a decrease in oxygen consumption was observed in the presence of CdSe NPs, particularly with NP8. This result is in accordance with a recent study showing a decrease in respiration when a bacterial community was subjected to TiO_2 NPs in an aerobic-sequencing batch reactor [67]. As several proteins involved in oxidation-reduction processes and DNA repair were down-regulated in the presence of NPs (e.g., catalase HPII with NP8; monooxygenase, NtaA/SnaA/SoxA family with NP8; DNA mismatch repair protein MutS with NP3; formaldehyde dehydrogenase, glutathione-independent with NP3 and NP8), a decrease in respiration could be a strategy adopted by *P. fluorescens* BA3SM1 to reduce H_2O_2 production and fight more easily oxidative stress in order to ensure a long-term survival during stationary growth phase. The stationary phase is a very complex state regulated by a variety of environmental and physiological cues [55]. During this phase, bacteria must deal with numerous stresses including nutrient starvation and the presence of NPs represents an additional stress. However, the decrease in respiration could also be directly induced by NPs. Indeed, authors suspected the smaller NPs to penetrate the bacterial cell membrane and inhibit respiratory enzymes [28].

In our experimental conditions, NP8 induced a large decrease in pyoverdine secretion (93%) and the down-regulation of proteins involved in iron binding and transport (e.g., TonB2 protein; TonB-dependent outer membrane copper receptor; outer membrane porins; siderophore-interacting protein). These results highlight that NP8 strongly affected several iron acquisition systems of *P. fluorescens* BA3SM1. Since the pyoverdine secretion was not impacted by 0.42 mg Se/L and less affected by 0.60 mg Cd/L than by NP8, we can suggest that the decrease in pyoverdine secretion observed with NP8 treatment was provoked by NPs rather than by metal ions released from these NPs. An inhibition in the pyoverdine secretion by NPs was also reported in several recent studies [68,69,70]. The siderophore pyoverdine plays a key role in microbial ecology as it drives bacterial survival and competitiveness in ecosystems. It is a significant factor for maintaining the habitats for most bacteria (for a review, see [29]). Besides, pyoverdine is also employed as a virulence factor in human pathogenic strains such as *P. aeruginosa* [71] and has important applications in the fight against antibiotic-resistant bacteria (for a review, see [29]). Consequently, our results highlight that NP8 can impact the secondary metabolism of bacteria with environmental and medical implications. However, by reducing the iron import, bacterial cells can more easily regulate pools of free iron and avoid an additional oxidative stress.

Proteomic analyses have shown that CdSe NPs induced numerous modifications in the composition and organization of cell envelope. For example, in the presence of NP8, we have observed a down-regulation of numerous membrane transporters suggesting that they play a major role as the gateway to NPs, forcing bacteria to reduce their numbers to stop the NP influx into the cells. This hypothesis is supported by

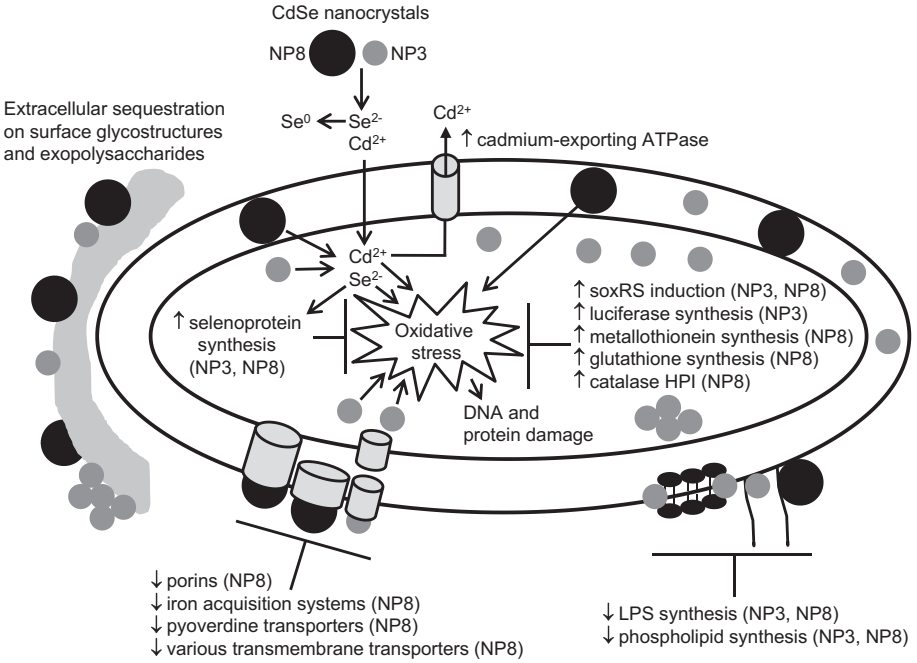

Fig. 7. Schematic representation of a major impact of CdSe colloidal nanocrystals (CdSe NPs) on *Pseudomonas fluorescens* BA3SM1. CdSe colloidal nanocrystals of 3 nm in diameter (NP3, small grey circles) and 8 nm in diameter (NP8, big black circles) are able to penetrate into the cell envelope causing important damage. NP3 are also capable to reach the cytoplasm. Cd^{2+} and Se^{2-} are released from CdSe NPs and enter the cell easily. CdSe NPs, Cd^{2+} and Se^{2-} probably induce an oxidative stress leading to DNA and protein damage. All these processes generate a major transcriptional response leading to 1) an active efflux of Cd^{2+}; 2) a high synthesis of exopolysaccharides and glycostructures to sequester CdSe NPs and facilitate biofilm formation; 3) an effective combat against oxidative stress thanks to soxRS regulatory system, luciferase, metallothioneins, glutathione, catalase HPI and selenoproteins; 4) a decrease in numerous transmembrane transporters and iron acquisition systems, probably to stop CdSe NP penetration into envelope and inside the cell; 5) a decrease in LPS (lipopolysaccharides) and phospholipids synthesis probably to reduce adsorption and aggregation of CdSe NPs on envelope components.

STEM images showing a concentration of NP8 around the cells and very few NP8 into cell envelope. The down-synthesis of major membrane transporters in the presence of NPs was also reported in a previous study [26]. NPs induced the down-regulation of several proteins involved in the synthesis of envelope components such as undecaprenyl-phosphate 4-deoxy-4-formamido-L-arabinose transferase (with NP3 and NP8) and CDP-diacylglycerol: serine O-phosphatidyltransferase (with NP3 and NP8). The undecaprenyl-phosphate 4-deoxy-4-formamido-L-arabinose transferase is implicated in the lipopolysaccharide (LPS) biosynthesis and the CDP-diacylglycerol: serine O-phosphatidyltransferase in the phospholipid biosynthesis. In recent studies, LPS and phospholipid groups were demonstrated to be involved in the adsorption and aggregation of NPs on Gram negative bacteria [72,73], thereby promoting the NP penetration into cell envelope and the disorganization of membranes. Consequently, our results seem to show that *P. fluorescens* BA3SM1 counteracts harmful effects of NPs on its envelope by reducing the synthesis of components allowing NP adsorption and aggregation such as LPS and phospholipids.

5. Conclusions

In our experimental conditions, NP3 formed numerous agglomerates and were able to penetrate *P. fluorescens* BA3SM1, while NP8 were highly concentrated around the bacteria, embedded in large exopolysaccharides. When this strain was exposed to NP3 and NP8 concentrations corresponding to a similar exchange surface area between NPs and bacterial cells for both treatments, the cell disorders were more numerous and more pronounced with NP8 than with NP3 (e.g., respiration decrease, growth retardation, a strong decrease in pyoverdine production and numerous changes in protein regulation). The stronger impact of NP8 could be explained by their higher volume, their higher metal content, their large concentration around bacterial cells and their low agglomeration maintaining an important exchange surface area and therefore a probably higher metal release. The lower impact of NP3 could be explained by their high agglomeration which leads to particles with fairly low surface to volume, and so, to a decrease in the exchange surface area. Hence, further study should be conducted to determine the cause of this aggregation. If it is mainly induced by NP-bacteria and NP-exopolysaccharides interactions, it seems interesting to deepen our understanding of these interactions to elucidate the mechanisms by which they contribute to NP agglomeration. Proteomic analyses revealed that the strain adapts to CdSe NPs by adopting essentially five defence mechanisms: cell aggregation, extracellular CdSe NP sequestration, effective protection against oxidative stress, modifications of envelope organization and properties, and cadmium export. A schematic representation of a major impact of CdSe NPs on *Pseudomonas fluorescens* BA3SM1 is shown in Fig. 7. The strain was able to sequester an equivalent of 1.6×10^{16} NP3/g dry weight and 1.7×10^{15} NP8/g dry weight, making it a promising agent for purifying waters contaminated by NPs via biofiltration processes.

Acknowledgements

The authors warmly thank Claire Guégan for her technical assistance.

This work was financially supported by the “Syndicat Mixte du Cotentin” (Aval 2013/397 - Des nanoparticules dans l'océan) and the “Conseil Régional de Basse-Normandie”(convention 2013 PCM 10 - NANOCEAN).

Appendix A. Supplementary data

Supplementary data to this article can be found online at http://dx.doi.org/10.1016/j.jprot.2016.07.021.

References

[1] W.J. Stark, P.R. Stoessel, W. Wohlleben, A. Hafner, Industrial applications of nanoparticles, Chem. Soc. Rev. 44 (2015) 5793–5805.
[2] A. Demortière, R.D. Schaller, T. Li, S. Chattopadhyay, G. Krylova, T. Shibata, P.C. dos Santos Claro, C.E. Rowland, J.T. Miller, R. Cook, B. Lee, E.V. Shevchenko, In situ optical and structural studies on photoluminescence quenching in CdSe/CdS/Au heterostructures, J. Am. Chem. Soc. 136 (2014) 2342–2350.
[3] Z. Gao, W. Jin, Y. Li, Q. Song, Y. Wang, K. Zhang, S. Wang, L. Dai, Flexible solar cells based on CdSe nanobelt/graphene Schottky junctions, J. Mater. Chem. C 3 (2015) 4511–4514.
[4] F. Hetsch, X. Xu, H. Wang, S.V. Kershaw, A.L. Rogach, Semiconductor nanocrystal quantum dots as solar cell components and photosensitizers: material, charge transfer, and separation aspects of some device topologies, J. Phys. Chem. Lett. 2 (2011) 1879–1887.
[5] K.V. Wong, N. Perilla, A. Paddon, Nanoscience and nanotechnology in solar cells, J. Energy Res. Technol. 136 (2014) 014001.
[6] Y.-H. Hsueh, W.-J. Ke, C.-T. Hsieh, K.-S. Lin, D.-Y. Tzou, C.-L. Chiang, ZnO nanoparticles affect *Bacillus subtilis* cell growth and biofilm formation, PLoS One 10 (2015), e0128457.
[7] S.S. Khan, S.S. Ghouse, P. Chandran, Toxic effect of environmentally relevant concentration of silver nanoparticles on environmentally beneficial bacterium *Pseudomonas putida*, Bioprocess Biosyst. Eng. 38 (2015) 1243–1249.
[8] R. Hardman, A toxicologic review of quantum dots: toxicity depends on physicochemical and environmental factors, Environ. Health Perspect. 114 (2006) 165–172.
[9] L. Wang, D.K. Nagesha, S. Selvarasah, M.R. Dokmeci, R.L. Carrier, Toxicity of CdSe nanoparticles in Caco-2 cell cultures, J. Nanobiotechnol. 6 (2008) 11–26.
[10] J.H. Priester, P.K. Stoimenov, R.E. Mielke, S.M. Webb, C. Ehrhardt, J.P. Zhang, G.D. Stucky, P.A. Holden, Effects of soluble cadmium salts versus CdSe quantum dots on the growth of planktonic *Pseudomonas aeruginosa*, Environ. Sci. Technol. 43 (2009) 2589–2594.
[11] J. Meng, Y. Ji, J. Liu, X. Cheng, H. Guo, W. Zhang, X. Wu, H. Xu, Using gold nanorods core/silver shell nanostructures as model material to probe biodistribution and toxic effects of silver nanoparticles in mice, Nanotoxicology 8 (2014) 686–696.
[12] C. Kirchner, T. Liedl, S. Kudera, T. Pellegrino, A. Muñoz Javier, H.E. Gaub, S. Stölzle, N. Fertig, W.J. Parak, Cytotoxicity of colloidal CdSe and CdSe/ZnS nanoparticles, Nano Lett. 5 (2005) 331–338.
[13] B.A. Rzigalinski, J.S. Strobl, Cadmium-containing nanoparticles: perspectives on pharmacology and toxicology of quantum dots, Toxicol. Appl. Pharmacol. 238 (2009) 280–288.
[14] A.M. Derfus, W.C.W. Chan, S.N. Bhatia, Probing the cytotoxicity of semiconductor quantum dots, Nano Lett. 4 (2004) 11–18.
[15] C. Zeng, A. Ramos-Ruiz, J.A. Field, R. Sierra-Alvarez, Cadmium telluride (CdTe) and cadmium selenide (CdSe) leaching behavior and surface chemistry in response to pH and O_2, J. Environ. Manag. 154 (2015) 78–85.
[16] M. Green, E. Howman, Semiconductor quantum dots and free radical induced DNA nicking, Chem. Commun. 1 (2005) 121–123.
[17] B.I. Ipe, M. Lehnig, C.M. Niemeyer, On the generation of free radical species from quantum dots, Small 1 (2005) 706–709.
[18] A. Valipoor, K. Parivar, M. Modaresi, M. Messripour, In vivo effects of quantum dot on organs development before maturity, Nanomed. J. 1 (2014) 258–265.
[19] A. Louvado, N.C.M. Gomes, M.M.Q. Simões, A. Almeida, D.F.R. Cleary, A. Cunha, Polycyclic aromatic hydrocarbons in deep sea sediments: microbe–pollutant interactions in a remote environment, Sci. Total Environ. 526 (2015) 312–328.
[20] D. Rosado, J. Usero, J. Morillo, Assessment of heavy metals bioavailability and toxicity toward *Vibrio fischeri* in sediment of the Huelva estuary, Chemosphere 153 (2016) 10–17.
[21] I. Poirier, P. Hammann, L. Kuhn, M. Bertrand, Strategies developed by the marine bacterium *Pseudomonas fluorescens* BA3SM1 to resist metals: a proteome analysis, Aquat. Toxicol. 128–129 (2013) 215–232.
[22] I. Poirier, L. Kuhn, C. Caplat, P. Hammann, M. Bertrand, The effect of cold stress on the proteome of the marine bacterium *Pseudomonas fluorescens* BA3SM1 and its ability to cope with metal excess, Aquat. Toxicol. 157 (2014) 120–133.
[23] I. Poirier, N. Jean, J.C. Guary, M. Bertrand, Robustness of cell disruption of heavy metal-resistant *Pseudomonas fluorescens* BA3SM1 isolates, Environ. Eng. Sci. 26 (2009) 1451–1457.
[24] F.A. Nejad, R.S. Riseh, P. Khodaygan, R. Ranjbar-Karimi, Biological control of take-all disease by isolates of *Pseudomonas fluorescens* and biosynthesis of silver nanoparticles by the culture supernatant of *Pseudomonas fluorescens* CHAO, Arch. Phytopathol. Plant Protect. 47 (2014) 1752–1763.
[25] J.R. Morones, J.L. Elechiguerra, A. Camacho, K. Holt, J.B. Kouri, J.T. Ramírez, M.J. Yacaman, The bactericidal effect of silver nanoparticles, Nanotechnology 16 (2005) 2346–2353.
[26] J.P. Monrás, B. Collao, R.C. Molina-Quiroz, G.A. Pradenas, L.A. Saona, V. Durán-Toro, N. Órdenes-Aenishanslins, F.A. Venegas, D.E. Loyola, D. Bravo, I.L. Calderón, C.C. Vásquez, T.G. Chasteen, D.A. Lopez, J.M. Pérez-Donoso, Microarray analysis of the *Escherichia coli* response to CdTe-GSH quantum dots: understanding the bacterial toxicity of semiconductor nanoparticles, BMC Genomics 15 (2014) 1099.
[27] I. Poirier, N. Jean, J.C. Guary, M. Bertrand, Responses of the marine bacterium *Pseudomonas fluorescens* to an excess of heavy metals: physiological and biochemical aspects, Sci. Total Environ. 406 (2008) 76–87.
[28] A. Kumar, A.K. Pandey, S.S. Singh, R. Shanker, A. Dhawan, Engineered ZnO and TiO_2 nanoparticles induce oxidative stress and DNA damage leading to reduced viability of *Escherichia coli*, Free Radic. Biol. Med. 51 (2011) 1872–1881.
[29] M. Saha, S. Sarkar, B. Sarkar, B.K. Sharma, S. Bhattacharjee, P. Tribedi, Microbial siderophores and their potential applications: a review, Environ. Sci. Pollut. Res. 23 (2016) 3984–3999.

[30] C. Romilly, C. Lays, A. Tomasini, I. Caldelari, Y. Benito, P. Hammann, T. Geissmann, S. Boisset, P. Romby, F. Vandenesch, A non-coding RNA promotes bacterial persistence and decreases virulence by regulating a regulator in *Staphylococcus aureus*, PLoS Pathog. 10 (2014), e1003979.
[31] H. Thiele, J. Glandorf, P. Hufnagel, Bioinformatics strategies in life sciences: from data processing and data warehousing to biological knowledge extraction, J. Integr. Bioinform. 7 (2010) 141.
[32] J.A. Vizcaíno, A. Csordas, N. del-Toro, J.A. Dianes, J. Griss, I. Lavidas, G. Mayer, Y. Perez-Riverol, F. Reisinger, T. Ternent, Q.-W. Xu, R. Wang, H. Hermjakob, 2016 update of the PRIDE database and its related tools, Nucleic Acids Res. 44 (2016) D447–D456.
[33] M. Sun, Q. Yu, M. Liu, X. Chen, Z. Liu, H. Zhou, Y. Yuan, L. Liu, M. Li, C. Zhang, A novel toxicity mechanism of CdSe nanoparticles to *Saccharomyces cerevisiae*: enhancement of vacuolar membrane permeabilization (VMP), Chem. Biol. Interact. 220 (2014) 208–213.
[34] S. Luche, E. Eymard-Vernain, H. Diemer, A. Van Dorsselaer, T. Rabilloud, C. Lelong, Zinc oxide induces the stringent response and major reorientations in the central metabolism of *Bacillus subtilis*, J. Proteomics 135 (2016) 170–180.
[35] S. Zarco-Fernández, A.M. Coto-García, R. Muñoz-Olivas, J. Sanz-Landaluze, S. Rainieri, C. Cámara, Bioconcentration of ionic cadmium and cadmium selenide quantum dots in zebrafish larvae, Chemosphere 148 (2016) 328–335.
[36] H.E. Pace, E.K. Lesher, J.F. Ranville, Influence of stability on the acute toxicity of CdSe/ZnS nanocrystals to *Daphnia magna*, Environ. Toxicol. Chem. 29 (2010) 1338–1344.
[37] T. Limcharoensuk, N. Sooksawat, A. Sumarnrote, T. Awutpet, M. Kruatrachue, P. Pokethitiyook, C. Auesukaree, Bioaccumulation and biosorption of Cd^{2+} and Zn^{2+} by bacteria isolated from a zinc mine in Thailand, Ecotoxicol. Environ. Saf. 122 (2015) 322–330.
[38] H. Maalej, N. Hmidet, C. Boisset, L. Buon, A. Heyraud, M. Nasri, Optimization of exopolysaccharide production from *Pseudomonas stutzeri* AS22 and examination of its metal-binding abilities, J. Appl. Microbiol. 118 (2015) 356–367.
[39] D.P. Higham, P.J. Sadler, M.D. Scawen, Cadmium-binding proteins in *Pseudomonas putida*: pseudothioneins, Environ. Health Perspect. 65 (1986) 5–11.
[40] M.-J. Kim, B.C. Lee, K.Y. Hwang, V.N. Gladyshev, H.-Y. Kim, Selenium utilization in thioredoxin and catalytic advantage provided by selenocysteine, Biochem. Biophys. Res. Commun. 461 (2015) 648–652.
[41] K. Helbig, C. Grosse, D.H. Nies, Cadmium toxicity in glutathione mutants of *Escherichia coli*, J. Bacteriol. 190 (2008) 5439–5454.
[42] C.-Y. Hsieh, M.-H. Tsai, D.K. Ryan, O.C. Pancorbo, Toxicity of the 13 priority pollutant metals to *Vibrio fisheri* in the Microtox® chronic toxicity test, Sci. Total Environ. 320 (2004) 37–50.
[43] M. Bebien, J.-P. Chauvin, J.-M. Adriano, S. Grosse, A. Vermeglio, Effect of selenite on growth and protein synthesis in the phototrophic bacterium *Rhodobacter sphaeroides*, Appl. Environ. Microbiol. 67 (2001) 4440–4447.
[44] C. Cuny, M. Lesbats, S. Dukan, Induction of a global stress response during the first step of *Escherichia coli* plate growth, Appl. Environ. Microbiol. 73 (2007) 885–889.
[45] M. Giró, N. Carrillo, A.R. Krapp, Glucose-6-phosphate dehydrogenase and ferredoxin-in-NADP(H) reductase contribute to damage repair during the soxRS response of *Escherichia coli*, Microbiology 152 (2006) 1119–1128.
[46] C. Cassier-Chauvat, F. Chauvat, Function and regulation of ferredoxins in the cyanobacterium, *Synechocystis* PCC6803: recent advances, Life 4 (2014) 666–680.
[47] H. Szpilewska, A. Czyż, G. Węgrzyn, Experimental evidence for the physiological role of bacterial luciferase in the protection of cells against oxidative stress, Curr. Microbiol. 47 (2003) 379–382.
[48] M.D. Rolfe, C.J. Rice, S. Lucchini, C. Pin, A. Thompson, A.D.S. Cameron, M. Alston, M.F. Stringer, R.P. Betts, J. Baranyi, M.W. Peck, J.C.D. Hinton, Lag phase is a distinct growth phase that prepares bacteria for exponential growth and involves transient metal accumulation, J. Bacteriol. 194 (2012) 686–701.
[49] G.K. Andrews, Regulation of metallothionein gene expression by oxidative stress and metal ions, Biochem. Pharmacol. 59 (2000) 95–104.
[50] J. Lemire, C. Auger, A. Bignucolo, V.P. Appanna, V.D. Appanna, Metabolic strategies deployed by *Pseudomonas fluorescens* to combat metal pollutants: biotechnological prospects, in: A. Méndez-Vilas (Ed.), Current Research, Technology and Education Topics in Applied Microbiology and Microbial Biotechnology, Formatex, Badajoz, Spain 2010, pp. 177–187.
[51] L.C. Seaver, J.A. Imlay, Hydrogen peroxide fluxes and compartmentalization inside growing *Escherichia coli*, J. Bacteriol. 183 (2001) 7182–7189.
[52] K. Kobayashi, M. Fujikawa, T. Kozawa, Oxidative stress sensing by the iron–sulfur cluster in the transcription factor, SoxR, J. Inorg. Biochem. 133 (2014) 87–91.
[53] A.J. Moyano, R.A. Tobares, Y.S. Rizzi, A.R. Krapp, J.A. Mondotte, J.L. Bocco, M.-C. Saleh, N. Carrillo, A.M. Smania, A long-chain flavodoxin protects *Pseudomonas aeruginosa* from oxidative stress and host bacterial clearance, PLoS Genet. 10 (2014), e1004163.
[54] Y. Zhu, J. Sun, Y. Zhu, L. Wang, B. Qi, Endogenic oxidative stress response contributes to glutathione over-accumulation in mutant *Saccharomyces cerevisiae* Y518, Appl. Microbiol. Biotechnol. 99 (2015) 7069–7078.
[55] J.M. Navarro Llorens, A. Tormo, E. Martínez-García, Stationary phase in gram-negative bacteria, FEMS Microbiol. Rev. 34 (2010) 476–495.
[56] C.O. Dimkpa, A. Calder, D.W. Britt, J.E. McLean, A.J. Anderson, Responses of a soil bacterium, *Pseudomonas chlororaphis* O6 to commercial metal oxide nanoparticles compared with responses to metal ions, Environ. Pollut. 159 (2011) 1749–1756.
[57] E.T.E. Niba, Y. Naka, M. Nagase, H. Mori, M. Kitakawa, A genome-wide approach to identify the genes involved in biofilm formation in *E. coli*, DNA Res. 14 (2007) 237–246.
[58] A. Kumar, S.K. Sarkar, D. Ghosh, A.S. Ghosh, Deletion of penicillin-binding protein 1b impairs biofilm formation and motility in *Escherichia coli*, Res. Microbiol. 163 (2012) 254–257.
[59] I.L. Mainprize, J.D. Bean, C. Bouwman, M.S. Kimber, C. Whitfield, The UDP-glucose dehydrogenase of *Escherichia coli* K-12 displays substrate inhibition by NAD that is relieved by nucleotide triphosphates, J. Biol. Chem. 288 (2013) 23064–23074.
[60] S. Koechler, J. Farasin, J. Cleiss-Arnold, F. Arsène-Ploetze, Toxic metal resistance in biofilms: diversity of microbial responses and their evolution, Res. Microbiol. 166 (2015) 764–773.
[61] B. García-Lara, M.Á. Saucedo-Mora, J.A. Roldán-Sánchez, B. Pérez-Eretza, M. Ramasamy, J. Lee, R. Coria-Jimenez, M. Tapia, V. Varela-Guerrero, R. García-Contreras, Inhibition of quorum-sensing-dependent virulence factors and biofilm formation of clinical and environmental *Pseudomonas aeruginosa* strains by ZnO nanoparticles, Lett. Appl. Microbiol. 61 (2015) 299–305.
[62] K. Ikuma, A.W. Decho, B.L.T. Lau, When nanoparticles meet biofilms-interactions guiding the environmental fate and accumulation of nanoparticles, Front. Microbiol. 6 (2015) 591.
[63] S.S. Khan, A. Mukherjee, N. Chandrasekaran, Adsorptive removal of silver nanoparticles (SNPs) from aqueous solution by *Aeromonas punctata* and its adsorption isotherm and kinetics, Colloids Surf. B: Biointerfaces 92 (2012) 156–160.
[64] M. Jakubiak, I. Giska, M. Asztemborska, G. Bystrzejewska-Piotrowska, Bioaccumulation and biosorption of inorganic nanoparticles: factors affecting the efficiency of nanoparticle mycoextraction by liquid-grown mycelia of *Pleurotus eryngii* and *Trametes versicolor*, Mycol. Prog. 13 (2014) 525–532.
[65] C. Auger, S. Han, V.P. Appanna, S.C. Thomas, G. Ulibarri, V.D. Appanna, Metabolic reengineering invoked by microbial systems to decontaminate aluminum: implications for bioremediation technologies, Biotechnol. Adv. 31 (2013) 266–273.
[66] R. Branco, T. Sousa, A.P. Piedade, P.V. Morais, Immobilization of *Ochrobactrum tritici* As5 on PTFE thin films for arsenite biofiltration, Chemosphere 146 (2016) 330–337.
[67] C. Supha, Y. Boonto, M. Jindakaraked, J. Ananpattarachai, P. Kajitvichyanukul, Long-term exposure of bacterial and protozoan communities to TiO_2 nanoparticles in an aerobic-sequencing batch reactor, Sci. Technol. Adv. Mater. 16 (2015) 034609.
[68] A. Mohanty, L. Wei, L. Lu, Y. Chen, B. Cao, Impact of sublethal levels of single-wall carbon nanotubes on pyoverdine production in *Pseudomonas aeruginosa* and its environmental implications, Environ. Sci. Technol. Lett. 2 (2015) 105–111.
[69] C.O. Dimkpa, J.E. Mclean, D.W. Britt, A.J. Anderson, CuO and ZnO nanoparticles differently affect the secretion of fluorescent siderophores in the beneficial root colonizer, *Pseudomonas chlororaphis* O6, Nanotoxicology 6 (2012) 635–642.
[70] C.O. Dimkpa, J.E. McLean, D.W. Britt, W.P. Johnson, B. Arey, A.S. Lea, A.J. Anderson, Nanospecific inhibition of pyoverdine siderophore production in *Pseudomonas chlororaphis* O6 by CuO nanoparticles, Chem. Res. Toxicol. 25 (2012) 1066–1074.
[71] I.L. Lamont, P.A. Beare, U. Ochsner, A.I. Vasil, M.L. Vasil, Siderophore-mediated signaling regulates virulence factor production in *Pseudomonas aeruginosa*, Proc. Natl. Acad. Sci. 99 (2002) 7072–7077.
[72] W. Jiang, K. Yang, R.W. Vachet, B. Xing, Interaction between oxide nanoparticles and biomolecules of the bacterial cell envelope as examined by infrared spectroscopy, Langmuir 26 (2010) 18071–18077.
[73] C. Yang, H. Xie, Q.-C. Li, E.-J. Sun, B.-L. Su, Adherence and interaction of cationic quantum dots on bacterial surfaces, J. Colloid Interface Sci. 450 (2015) 388–395.